Investigating the Impact of Ice Formation on Winter Discharge Fluctuations in the Dischmàbach

---

GEO 511 - Master's Thesis

Supervised by
Michael Margreth, WSL
Dr. David Vetsch, VAW ETHZ
Prof. Dr. Jan Seibert, UZH

Submitted by
Nina Nagel
Mat. Nr. 17-734-591

November 6, 2023

Department of Geography, University of Zurich

Abstract

Oscillations and anomalies in low-flow discharge hydrographs are frequently misinterpreted as artifacts or data inaccuracies, even when some variations are genuinely due to natural stream events. For instance, temporary river ice formations during severe winter conditions can induce variations in discharge, manifested as drops followed by peaks in the hydrograph. Such a phenomenon, where ice buildup overnight halts water flow until it breaks and releases the next day, was noted in the Dischmàbach near Davos. This study delves into the causes of discharge oscillations during winter, focusing on the Dischmàbach as a case study. A field survey conducted in Winter 2022-2023 assessed stream ice formations and the accompanying changes in discharge. This was done using stationary wildlife cameras, water level sensors, temperature loggers, and drone surveys, complemented by data from the Federal Office of Environment (FOEN). Subsequent exploratory analysis involved characterizing stream morphology at ice-rich locations in the creek, particularly at three specific case locations. An algorithm has been developed that scrutinizes the hydrograph to pinpoint ice formation events and ascertain the volume of water retained during these icing events. Drone surveys were employed to map ice locations along the stream and estimate the volume of retained water. Findings indicate that temporary ice formations are prevalent in stream sections with typical pool and step morphology, where the river gradient transitions from flat to steep. Such locations are marked by turbulent flow, abundant boulders, and variations in slope and width. Ice events identified in the hydrograph revealed that nearly half of the winter discharge oscillations result from these temporary ice formations. Furthermore, historical discharge measurements of the Dischmàbach only sporadically showed ice-induced hydrograph patterns, even during one of the coldest winters recorded over the past 19 years. This absence suggests that oscillations may have been mistakenly eliminated through manual corrections.

Acknowledgments

This thesis received generous funding from the Swiss Federal Institute for Forest, Snow and Landscape Research (WSL) and the Federal Office for the Environment (FOEN), to whom I extend my deepest gratitude.

Firstly, my sincere thanks go to Florian Lustenberger, research assistant at WSL, not only for his pivotal role in crafting the new data analysis algorithm but also for his invaluable assistance during our fieldwork.

Secondly, orchestrating the field campaign and measurement was no small feat, and it would not have been possible without the dedication of many. In this regard, I wish to express my gratitude to Stefan Boss, Roman Ackle, Florian Lustenberger, and Raphael Moser, research staff from WSL and VAW (Laboratory of Hydraulics, Hydrology and Glaciology), for their indispensable technical expertise during the installation and deployment of field instrumentation. My appreciation also extends to Jana von Freyberg, Michael Plüss, and Christian Rickli, research staff from WSL and EAWAG (Swiss Federal Institute of Acquatic Science and Technology) who generously provided the sensors and cameras essential for this work.

A special acknowledgment is due to Thomas Fankhauser, the retired gamekeeper in the Dischma Valley. His assistance in the field and his captivating stories about the valley added a rich layer of understanding to my work.

Furthermore, the contribution of Yves Bühler and Andreas Stoffel from the Institute for Snow and Avalanche Research (SLF) has been instrumental. Their meticulous work on the drone flights and subsequent processing of the raw ortho and DSM images significantly enriched this thesis.

I'm grateful to Andreas Kohler, the representative of the FOEN hydrological department. Our insightful meeting shed light on the intricacies of hydrological data management by the authorities, offering a fresh perspective to my study.

I would be remiss not to mention the unwavering emotional support I received from my friends and family. Their encouragement and willingness to peer-review my work were both sources of strength and motivation.

Lastly, I thank my supervisors, Michael Margreth - PhD candidate at WSL, and Dr. David Florian Vetsch, lecturer and head of the research group *Numerical Modelling* at VAW. Their guidance and unwavering support were the linchpins of this journey. Additionally, I'm deeply grateful to Prof. Dr. Jan Seibert, Head of the Hydrology and Climate Department at the University of Zurich, for his instrumental insights, greatly enhancing my research overview throughout this endeavor.

Contents

1 Introduction **1**

1.1 Related work . . . 2

1.1.1 A general introduction to low-flow hydrology . . . 2

1.1.2 Low-flow in alpine catchments . . . 4

1.1.3 River ice processes . . . 4

1.1.3.1 Ice formation in small rivers: supercooling, frazil ice, and anchor ice . . . 5

1.1.3.2 Anchor ice . . . 7

1.1.3.3 River morphology . . . 8

1.2 Research gaps . . . 9

1.3 Research questions . . . 9

1.4 Thesis procedure . . . 10

2 Study Site **11**

3 Data **13**

3.1 Fieldwork-data . . . 13

3.1.1 Measured Variables . . . 13

3.1.2 Sensor/Device Placement . . . 14

3.1.2.1 Wildlife cameras . . . 16

3.1.2.2 Water temperature loggers . . . 17

3.1.2.3 Drone flights . . . 17

3.1.2.4 Water-stage and water temperature sensors . . . 18

3.2 FOEN-Data . . . 19

4 Methods **21**

4.1 Morphological analysis of stream ice formation dynamics . . . 22

4.1.1 Morphological characterization of the Dischmàbach . . . 22

4.1.2 Morphological characterization of the Pools . . . 23

4.2 Event analysis . . . 24

4.2.1 Ground Truth: Event characterization . . . 24

4.2.2 Event extraction procedure . . . 25

4.2.2.1 Step 1: Event finding . . . 25

4.2.2.2 Step 2: No-Ice-Model . . . 25
4.2.2.3 Step 3: Intersection Points . . . 26
4.2.2.4 Calculated parameters . . . 28
4.2.3 Model validation . . . 29
4.3 Event-specific analysis utilizing drone images . . . 29

5 Results **30**
5.1 Morphological analysis of stream ice formation dynamics . . . 30
5.1.1 Stream morphology . . . 30
5.1.2 Pool morphology . . . 32
5.1.2.1 Pool 1 . . . 32
5.1.2.2 Pool 2 . . . 35
5.1.2.3 Pool 3 . . . 36
5.2 Event analysis . . . 39
5.2.1 Event characterization . . . 39
5.2.2 Validation . . . 39
5.2.3 Events and volume analysis results . . . 42
5.2.3.1 Winter 2022-2023 . . . 42
5.2.3.2 Winter 2005-2006 and winter 2021-2022 . . . 45
5.3 Event-specific analysis utilizing drone images . . . 47
5.4 Stage sensor results . . . 49

6 Discussion **50**
6.1 Morphological analysis of stream ice formation dynamics . . . 50
6.1.1 Stream morphology . . . 50
6.1.2 Pool morphology . . . 51
6.1.3 Summed up discussion points to the morphological analysis of stream ice formation dynamics . . . 52
6.2 Event analysis . . . 53
6.2.1 Analysis of the Event-Finding-Algorithm Efficiency and Event Identification 53
6.2.1.1 Event characterization: . . . 53
6.2.1.2 Event-Finding-Algorithm performance: . . . 54
6.2.2 Evaluation of the Events and the Impounded Water Volumes . . . 54
6.2.2.1 Winter 2022-2023 . . . 54
6.2.2.2 Winter 2005-2006 and Winter 2021-2022 . . . 55
6.2.3 Summed up discussion points to the event analysis . . . 57
6.3 Results from drone images and comparison to the Event-Finding-Algorithm results 57
6.4 Evaluation of the stage sensor results . . . 58
6.5 Answering the research questions . . . 58
6.6 Uncertainties . . . 59

7 Conclusion **61**
7.1 Main achievements 62
7.2 Possible outlooks 62

8 Excursus **64**

9 Appendix **70**
9.1 Stream width calculation pseudocode 70
9.2 Event characterisation 71
9.3 Event extraction pseudocode 72
9.3.1 *Smooth spline* No-Ice-Model 72
9.3.2 *Exponential decay* No-Ice-Model 73

List of Figures

1.1 Water temperature (Tw) time series recorded in a laboratory tank being cooled by a constant surface heat flux to supercooling, from Boyd, T. Ghobrial, M. Loewen, et al., 2022, p. 2 . . . 6
1.2 Slush ice observed in the riverbed of the Dischmàbach, picture taken by Nina Nagel, 12.12.2022 . . . 7

2.1 Overview map of the Dischmàbach catchment created in QGIS with the geodata from Swisstopo . . . 12

3.1 Overview map of the Dischmàbach catchment created in QGIS, with the placement of the sensors and devices during the field campaign of the winter 2022-2023 15
3.2 Wildlife camera installed at Pool 1 (left), Pool 2 (middle) and Pool 3(right), pictures taken by Nina Nagel, 12.12.2022 . . . 16
3.3 Location of T-Logger 1 and T-Logger 2 in Pool 1, pictures taken by Nina Nagel, 30.11.2022 . . . 17
3.4 Location of T-Logger 3 and T-Logger 4 in Pool 3, pictures taken by Nina Nagel, 30.11.2022 . . . 17
3.5 Map overview with the covered areas by the drone flights . . . 18
3.6 Stage sensor nr. 6166 installed near Pool 1 (left), nr. 6300 near Am Rin (middle) and nr. 12443 near Dürrboden (right), pictures taken by Nina Nagel, 09.11.2022 and 07.02.2023 . . . 19

4.1 Sketch illustrating the step 3 procedure, drawn by Nina Nagel . . . 27

5.1 Elevation, width, and slope along the Dischmàbach measured/calculated for every 2 m and the locations showing a rise in the water level (red dots) . . . 31
5.2 Stream elevation and stream width along the Dischmàbach every 2 m around the location of Pool 1 (red area) and the locations showing a rise in the water level (red dots) . . . 33
5.3 Pool 1 the 12.12.2022 at 08:30 showing anchor ice formation and water retention, picture taken by Nina Nagel . . . 34
5.4 Pool 1 the 07.02.2023 with the ice cover over the stream, picture taken by Nina Nagel . . . 34

5.5 Pool 1 the 08.02.2023 during a freezing event and the ice cover over the stream, picture from the wildlife camera 34
5.6 Water Temperature in Pool 1 between December 2022 and March 2023, one near the morphological step (T-Logger 1) and the second further behind the morphological step (T-Logger 2) 35
5.7 Stream elevation and stream width along the Dischmàbach every 2 m around the location of Pool 2 (red area) and the locations showing a rise in the water level (red dots) 36
5.8 Pool 2 on the 21.03.2023 with no anchor ice formation and water retention, picture from the wildlife camera 36
5.9 Pool 2 on the 08.02.2023 with retention due to ice formation, picture from the wildlife camera 36
5.10 Stream elevation and stream width along the Dischmàbach every 2 m around the location of Pool 3 (red area) 37
5.11 Pool 3 on the 12.12.2022 not showing any ice formation that causes water retention, picture taken by Nina Nagel 38
5.12 Pool 3 the 08.02.2023 with no visible ice formations, screenshot from the drone flight ortho image 38
5.13 Water temperature in Pool 3 between December 2022 and March 2023 38
5.14 Overview of the found events by the algorithm with the *exponential decay* No-Ice-Model and a pre-time of 5 days with the events detected by the wildlife camera(red lines) 40
5.15 Overview of the found events by the algorithm with the *smooth spline* No-Ice-Model and a pre-time of 5 days the events detected by the wildlife camera(red lines) 41
5.16 Icing events found by the Event-Finding-Algorithm in winter 2022-2023 the events detected by the wildlife camera(red lines) 42
5.17 Resulting retention volumes due to ice in the Dischmàbach in comparison to the expected discharge from the No-Ice-Model 45
5.18 Icing events found by the Event-Finding-Algorithm in the winter 2005-2006, coldest winter between 2004 and 2023 46
5.19 Icing events found by the Event-Finding-Algorithm in the winter 2021-2022, warmest winter between 2004 and 2023 46
5.20 Pool 1 on the 08.02.2023, areal picture during an icing event with colored water surface elevation difference to the 20.02.2023 areal image, screenshot of the drone flight imagery 48
5.21 Pool 2 on the 08.02.2023, areal picture during an icing event with colored water surface elevation difference to the 20.02.2023 areal image, screenshot of the drone flight imagery 48

5.22 Measured water level with the Decentlab sensors in the top (Dürrboden), middle (Am Rin) and bottom (near Pool 1) of the valley 49

8.1 Discharge graph with the found event by the algorithm and the observed event with the wildlife camera (red line) and the moon phases (SpaceWeatherLive, 2023) 65

9.1 Characterization table of all the events found by the wildlife camera and additional statistics to define the threshold values for the Event-Finding-Algorithm divided into early (blue) and late (orange) winter 71
9.2 Air temperature ranges over the events found by the wildlife camera at different times during the day 72
9.3 Air temperature ranges over the events found by the wildlife camera at different times during the day, and the vertical line marking the change from early to late winter 72
9.4 Water temperature ranges over the events found by the wildlife camera at different times during the day, and the vertical line marking the change from early to late winter 72
9.5 Water temperature over different times during the day forthe events found by the wildlife camera 72

List of Tables

3.1 Collected data during fieldwork in winter 2022-2023* 13

5.1 Statistical parameters evaluating the stream morphology 32
5.2 Threshold values 39
5.3 Total event count of the No-Ice-Models over the winter 2022-2023 39
5.4 Number of events detected by the No-Ice-Models matching the ground truth event count (tot. 15) over the Winter 2022-2023 40
5.5 Calculated volumes with the Event-Finding-Algorithm 44
5.6 Threshold values for the data from 2004 to 2022 45
5.7 Summed volumes and mean volumes retained by the ice in comparison to all negative discharge fluctuations in winter for the case study and the warmest (2021-2022) and coldest (2005-2006) winter in the last 19 years 47
5.8 Calculated volumes of water retained due to ice with the drone flight imagery . . 48

6.1 Comparison of air temperature thresholds observed in different field studies investigating ice formations in streams 53

Chapter 1

Introduction

An in-depth understanding of alpine hydrologic systems forms a linchpin in hydrologic research, mainly due to their central role in water supply and management in Europe, where they are often dubbed the "water castle of Europe" (FOEN, 2021). This central position establishes them as a primary source for diverse water-related applications, including resource management, risk assessment, and drought assessment. As a result, natural water dynamics in high alpine areas are becoming the focus of numerous research questions and investigations. Swiss authorities consider this topic an essential area to be regularly updated and further researched (FOEN, 2021). In addition, alpine rivers are in a direct and complex interplay with various processes such as snowfall, glacier melt, permafrost, and spring water, all of which together form a multi-faceted system that requires in-depth study and understanding (Verbunt et al., 2003).

In hydrological research, there is considerable focus on studying various river flow dynamics, essential to understanding water movement and catchment interplay in different geographic and climatic contexts (Verbunt et al., 2003). A key aspect of this research field is the detailed study of low-flow phases of rivers, which manifest as recurring periods within a year where the river discharge shows the lowest annual values. Understanding low-flow conditions in rivers is crucial, especially when determining how much water can be utilized versus how much should remain in the rivers. Based on this understanding, various laws geared toward water protection and fish habitat conservation have been established. For instance, in Switzerland, a law has been enforced to ensure watercourses maintain their natural functions. To achieve this, a sufficient amount of water must remain in river and stream beds downstream of water withdrawals (FOEN, 2022). This requisite volume is determined using the Q_{347} metric, which represents the discharge that is expected to be equaled or exceeded on an average of 347 days in a year. It provides a standardized benchmark to ensure adequate water flow for ecological and environmental purposes, even during periods of lower river discharge (BUWAL, 2000). For alpine rivers, the low-flow period mainly occurs in winter[1], where the discharge slowly depletes until the first snow melts

[1] In this thesis, winter is primarily referred to the cold season of the year, which overlaps in fall as well as in spring and starts around November until the end of March.

in spring (Schaefli, Rinaldo, and Botter, 2013). However, the winter phase is less studied due to the dominating snow dynamics. During this time, river discharge dynamics tend to take a back seat, as waterways are often blocked by ice and snow, making them less accessible for investigation (Schaefli, Rinaldo, and Botter, 2013). In addition, winter conditions make it challenging to access high-elevation areas, significantly hindering or even making fieldwork in many research projects impossible. In hydrological research, efforts are made to study the complex hydraulic cycle of a high mountain river in winter. In this framework, the research project of M. Margreth[2] during his doctoral thesis, he has initiated a specialized study of the recession behavior of alpine waters. During the measurement campaigns of this project, it was found that the winter discharge hydrograph of an alpine river has specific anomalies that complicate the study of recession behavior. Alpine watercourses frequently showed daily fluctuations and anomalies in the hydrograph during the winter months. Anomalies observed in hydrographs during low-flow periods are frequently misconstrued or erroneously ascribed to malfunctions in measurement instruments. However, it is essential to recognize that such anomalies may not necessarily result from device malfunctions; they might instead require deeper investigation to gain a more comprehensive understanding of their underlying causes (Strohmenger et al., 2023). Notably, specific deviations in the low-flow data of Alpine rivers were promptly attributed to freezing conditions, prompting subsequent examination and analysis.

This thesis focuses on river ice dynamics in the case study of the Dischmàbach in Davos, Switzerland. The aim is to understand the process of river ice formation in more detail and to relate it to winter runoff behavior for this case study. This approach starts with an in-depth analysis of the basic principles, based on which strategies can be developed to allow a more efficient investigation of low-flow phases in alpine streams.

1.1 Related work

In the following section, a review of relevant literature and studies is undertaken to establish a foundational understanding of the central concepts of this research. Key terms and processes are introduced and delineated, facilitating a deeper comprehension of the subsequent analyses. This encompasses examining rivers' low-flow and recession behaviors and exploring the physical processes governing river ice formation. The intention is to pinpoint existing gaps in current research, thereby framing the context for the ensuing study.

1.1.1 A general introduction to low-flow hydrology

Low-flow hydrology represents a prominent research field in various hydrology or water resources management domains. In this context, low-flow is a recurring annual period during which the

[2]Michael Margreth is a PhD candidate at the Swiss Federal Institute for Forest, Snow and Landscape Research (WSL). His research focuses on developing a method for the determination of low water recession curves and their transfer to ungauged catchments.

lowest annual discharge occurs in a hydrological unit – such as a watershed and its rivers – due to prolonged scant precipitation. These periods are primarily fed by groundwater discharge, lake water discharge, peatlands, or glacial melt, characterized by a slowed water supply (Smakhtin, 2001). Low-flow periods vary considerably regarding climate and topography and can have differing durations. The interest in understanding low-flow properties lies in their significant importance for planning water resources, reservoir storage, or water quality (Smakhtin, 2001; Tallaksen, 1995). Another central concept is the base flow, which is determined by dissecting the hydrograph of a specific stream. The total runoff hydrograph is the sum of the base flow with the surface runoff, interflow, and quick flow (Gan, Sun, and Luo, 2015). In contrast to low-flow, base flow is not an annual period but rather represents the proportion of water in the river hydrograph that is released from slow reservoirs like groundwater, marshes, glacier melt, and lake water. Consequently, one could conclude that base flow constitutes a substantial part of a low-flow period (Smakhtin, 2001). Hydrology introduced the concept of recession to elucidate or quantify these terms. The recession curve plots the depletion of river discharge over a specific time frame. This trend usually takes the form of exponential decay, where the hydrograph initially exhibits high discharge values, consisting of quick flow, surface flow, and interflow, before the curve flattens and the base flow becomes the dominant component expressing through the base-flow-recession curve (Smakhtin, 2001; Tallaksen, 1995). Recession curves are a crucial tool in hydrology, providing comprehensive insights into a watershed's water budget dynamics - illustrating the relationship between the storage volume and the discharge in a catchment area. Moreover, integrating the recession curve enables an accurate estimation of the available drainage capacity (Smakhtin, 2001). It is essential to note that the individual recession curve of a river depends on various factors, such as the specific geology of the area, the characteristics of the local vegetation, the topography, and the regional climatic conditions. Therefore, it can be considered a unique feature of each river (Smakhtin, 2001). In scientific studies, various methods have been developed for constructing a master recession curve. This is formed by integrating numerous recession curves from low-flow periods over several years. This composite curve paints a general picture of the behavior of a water reservoir, thus facilitating an understanding of the specific characteristics of a watershed. Consequently, the master recession curve represents an indispensable tool for precise hydrological predictions (Smakhtin, 2001; Lamb and Beven, 1997). There is no universal method for precisely capturing recession curves; instead, various procedures and approaches differ in complexity and specific application areas (Fiorotto and Caroni, 2013). These methods rely on different mathematical and statistical systems developed to enhance the reliability and precision of curve determination. In scientific research, new techniques and models are continuously developed to refine these methods' accuracy further. This is part of a dynamic field of study that constantly evolves to address diverse watersheds' changing climatic conditions and hydrological characteristics (Posavec, Giacopetti, and Birk, 2017; Stoelzle, Stahl, and Weiler, 2013).

1.1.2 Low-flow in alpine catchments

In high-altitude areas such as the Alps, the low-flow season of a creek or river occurs mainly in winter to early spring before the snow melt season. This is due to snow precipitation, which is accumulating on the ground. In these mountainous regions, melt water from glaciers is reduced or completely absent during winter. Therefore, the rivers, unless they freeze entirely, are primarily fed by groundwater discharge or not fully frozen lake outflows (Smakhtin, 2001). In scientific studies, such catchment areas are often characterized as "*dormant*" during the winter since not much changes hydrologically (Schaefli, Rinaldo, and Botter, 2013). This implies that hydrological processes are slowed down at this time, and the dynamic interactions observed in other seasons are limited. Consequently, it is possible to calculate the recession curves of alpine streams mainly in winter. However, this season, the water is exposed to cold air temperatures, which may cause the water to freeze occasionally, producing some striking patterns in the data (*cf. doctoral Thesis of Michael Margreth, WSL*).

1.1.3 River ice processes

Ice processes in rivers are a natural phenomenon that has received increasing attention in the scientific literature since the 1960s and 1970s. This primarily pertains to regions in higher latitudes and areas with greater altitudes, where the climatic conditions permit low temperatures that characterize the cold season. Understanding river ice formations is essential, especially in large rivers used for navigation or dammed for electricity generation. River ice can substantially impede river traffic or electricity production. Ice jams and their sudden releases can trigger floods and other destructive events that humans must contend with (Chen et al., 2023; Blackburn and She, 2019). For this reason, this phenomenon has been extensively researched to understand it better and develop appropriate countermeasures. The increased interest in ice processes in rivers arose from practical applications and associated challenges and led to research into the natural causes and processes that control such phenomena (Beltaos, 2013). A deeper understanding of these driving forces not only enables better management in terms of navigation, flood management and power generation but also provides valuable insights into nature itself. Various elements determine river ice formation processes, including hydro-meteorological factors and the river's geometric, hydraulic, and thermal characteristics. For example, the type of ice regime depends in part on the slope angle of the river. Ice forms as sheets in rivers with gentle gradients, resulting from the accumulation and compaction of frazil slush and ice pans. Ice cover may be irregular in rivers with steep gradients, with anchor ice and overhanging ice barriers (Beltaos, 2013; Turcotte and Morse, 2013). In the past, the study of ice formation and its dynamics in streams has often focused on larger rivers, especially those with widths larger than 50 m. This was mainly because of the practical relevance and extensive impact of ice events in large watercourses. Nevertheless, smaller rivers warrant distinct attention regarding river ice (Buffin-Bélanger, Bergeron, and J. Dubé, 2013; T. R. Ghobrial and M. R. Loewen, 2021). They

are often found higher up in the watershed grade and typically at elevated terrains, where their geographic placement exposes them to colder environments (Barry, 1992). With their unique morphology and diverse flow characteristics, small rivers demonstrate a significant and variable hydrologic response to ice formation (Buffin-Bélanger, Bergeron, and J. Dubé, 2013). They are more prone to icing for several reasons. Their limited water volume equals a diminished heat capacity, and the high surface-to-volume ratios can lead to faster heat dissipation. Moreover, their untouched state, coupled with a distinct river morphology, is often accompanied by dense riparian vegetation which have an impact on the incoming solar radiation by giving more shadow (Buffin-Bélanger, Bergeron, and J. Dubé, 2013). It still needs to be considered that the water in such rivers often comes from underground groundwater sources. In many cases, these springs may have a more moderate water temperature, which affects the freezing tendency of the water. Given this complex interplay of factors, understanding the nuances influencing ice formation in these rivers becomes crucial (Buffin-Bélanger, Bergeron, and J. Dubé, 2013).

River ice formation, or ice accretion, begins in most streams by a similar process: fine ice crystals called frazil ice emerge at cold water temperatures. This frazil ice, consisting of tiny, needle-shaped ice crystals, is often transported by current movement along the river bank or bed, where it begins to deposit and accumulate. Over time and under suitable conditions, these accumulations can grow into larger ice structures, exerting considerable influence on river flow and hydraulics (Chen et al., 2023). In the following chapters, the complex process of ice accretion is discussed in detail based on scientific literature. Special attention is given to the characteristics and dynamics of smaller rivers, which often have unique ice formation processes due to their morphology and flow characteristics.

1.1.3.1 Ice formation in small rivers: supercooling, frazil ice, and anchor ice

River ice originates in turbulent, supercooled waters, predominantly when chilling air temperatures prevent ambient water warming. Ice crystals emerge and cluster in such environments, culminating in frazil ice (T. R. Ghobrial and M. R. Loewen, 2021). Driven by vertical mixing, these ice crystals often cling to specific points, notably the riverbed, evolving into "*anchor ice*". As this process unfolds, the ice may expand above the water's surface (Daly, 2013). The intricacies of these ice formation dynamics are delved into in subsequent subsections.

Supercooling If the heat flux at the water surface is persistently negative, supercooling of the water can occur in streams. This phenomenon occurs mainly under meteorological conditions when air temperatures drop below freezing. These circumstances typically manifest in temperate regions from late autumn, when water initiates the freezing process, to early spring (Boyd, T. Ghobrial, M. Loewen, et al., 2022). During this supercooling process, the water temperature can drop slightly below 0 °C, resulting in nucleation and formation of ice crystals in the water. Once the ice starts forming, the latent heat emitted counterbalances the cooling at the water surface,

causing the water temperature to approach 0 °C (McFarlane and Clark, 2021) (see Figure 1.1). Although these crystals tend to form near the water surface, they are displaced in the deeper water layer by vertical turbulence (Boyd, T. Ghobrial, M. Loewen, et al., 2022).

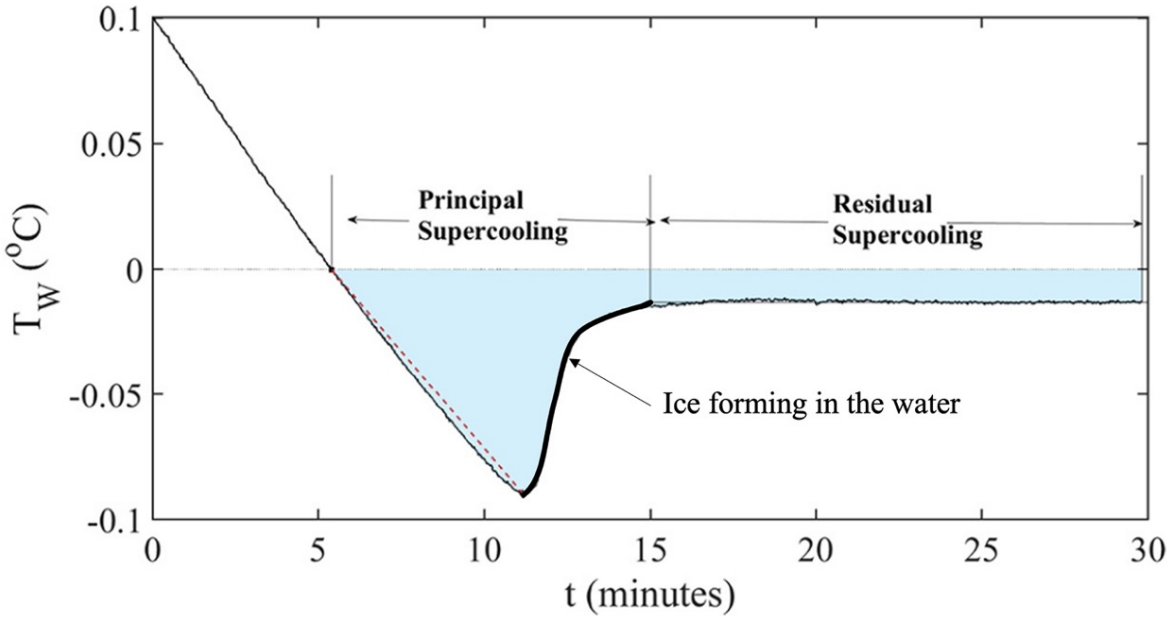

Figure 1.1: Water temperature (Tw) time series recorded in a laboratory tank being cooled by a constant surface heat flux to supercooling, from Boyd, T. Ghobrial, M. Loewen, et al., 2022, p. 2

A recent study by Boyd, T. Ghobrial, and M. Loewen, 2023 which analyzed supercooling events in Alberta, Canada, discovered that longwave radiation is the primary cause of negative heat flux. This radiation is predominantly emitted at night, leading to the presence of supercooled water mainly after the sun's last rays have set. In contrast, during the day, the short-wave radiation from the sun that strikes the water surface reverses the heat flux to positive. Consequently, the periodic occurrence of supercooling at both day and night intervals can influence river ice formations. This finding suggests that the breakup of ice is not solely influenced by air temperature but rather significantly determined by incoming radiation. Various research efforts have sought to identify the maximum air temperature at which the supercooled water phenomenon occurs. For example, the study by Boyd, T. Ghobrial, and M. Loewen, 2023 in Canada has determined that the critical temperature is -5.4 °C. In contrast, another Canadian study by K. Alfredsen, Stickler, and Pennell, 2006 set the threshold at -15 °C, while an older study from Japan by Terada, Hirayama, and Sasamolo, 1999 identified a maximum temperature of -10 °C as the threshold. From these divergent results, it can be concluded that the required air temperature must be in the negative range, although no universal threshold can be established. Regional climatic differences and specific characteristics of the respective river environments can explain this variance.

Frazil and anchor ice formation Within supercooled and turbulent water, frazil ice crystals nucleate near the water surface and disperse deeper into the water column through vertical

mixing. Frazil crystals in supercooled water are deemed “active” and possess a propensity to aggregate, forming frazil flocs. So-called nuclei or “seeds” are required to start the crystallization process in water. These act as the starting point for the growth of ice crystals. The seeds can come from different sources. These include tiny water droplets thrown onto the water surface by currents or microscopic particles in the environment where crystallization can begin. These nuclei are essential because they provide a surface on which water molecules can arrange themselves, thus initiating the crystallization process (Daly, 2013). Once the ice has formed, it may adhere to the riverbed and give rise to anchor ice formations, which seem to coat the stones in the riverbed in a white translucent foam (Qu and Doering, 2007) (Figure 1.2).

Figure 1.2: Slush ice observed in the riverbed of the Dischmàbach, picture taken by Nina Nagel, 12.12.2022

1.1.3.2 Anchor ice

The occurrence of anchor ice is typically observed in river reaches that contain a significant amount of bedload and substrate, as well as at natural weirs or widened areas of the river channel (Pan, Shen, and Jasek, 2020). Anchor ice exhibits a diurnal pattern, forming briefly during colder periods and dissipating as temperatures rise (Pan, Shen, and Jasek, 2020). It forms directly on the riverbed substrate and anchors itself to it. This attachment allows the buoyancy of the ice, in combination with static friction, to overcome the flow forces of the water

and allowing it to remain on the riverbed (Stickler and K. T. Alfredsen, 2009). The presence of anchor ice has a significant impact on the hydraulic characteristics of a river channel. Not only can it alter flow patterns, but it can also cause a localized rise in water level, reducing discharge and the flow velocity. Furthermore, anchor ice can reduce bottom roughness by adhering to and trapping substrate particles, affecting flow resistance. In addition, the formation and subsequent release of anchor ice can lead to morphological changes in the river section in question (Nafziger et al., 2017; M. Dubé, Turcotte, and Morse, 2014). In smaller streams, anchor ice plays a vital role concerning discharge dynamics. Due to their reduced discharge capacity, especially during the winter months, and their narrower river courses, even small accumulations of anchor ice can become significant obstacles to water flow. This can cause water to back up or even, in extreme cases, temporarily block the flow of the river. The resulting discharge changes can have short-term and long-term effects on river morphology, sediment transport and the surrounding ecosystem (Nafziger et al., 2017; M. Dubé, Turcotte, and Morse, 2014).

1.1.3.3 River morphology

The morphology of a river plays a crucial role in the formation of river ice, as not every section of a river experiences ice formation in the same manner (Turcotte and Morse, 2013; Pan, Shen, and Jasek, 2020). Numerous studies have documented that anchor ice preferably forms in areas with specific morphological characteristics, such as morphological steps, in riffle areas, or between emerging boulders (K. Alfredsen, Stickler, and Pennell, 2006). This formation occurs especially in turbulent water sections or transition zones between slow and fast water currents. This is because the characteristic water movement at these sites facilitates sufficient energy dissipation to generate a negative heat flux. This, in turn, promotes the formation of supercooled water, which serves as a starting point for ice formation (Turcotte and Morse, 2013; Stickler and K. T. Alfredsen, 2009; Nafziger et al., 2017; Hirayama, Yamazaki, and Tao Shen, 2002).

To deepen the understanding of the role of river morphology, a study by Turcotte and Morse, 2013 classified the various types of river ice depending on the channel morphology. In this process, the river's flow properties were analyzed in connection with the climatic conditions and assigned to different ice types. The slope of the river represents a significant factor. For instance, in a river with a step-pool morphology and a slope between 0.02 and 0.08 in a mild climate, suspended ice and "ice shells" are more likely to form. Anchor ice also falls into this category (Turcotte and Morse, 2013). An additional investigation conducted by Hirayama, Yamazaki, and Tao Shen, 2002 also found that such anchor ice dams can form in a stepped river course. It was observed that an optimal river slope should be between 0.001 and 0.02 to facilitate the formation of these ice structures.

1.2 Research gaps

From the above literature review, the following three research gaps were identified:

Relation between recession analysis and river ice: Recent research discussions provide a substantial foundation for understanding low-flow and recession and river ice dynamics. However, an evident gap in the current literature pertains to the explicit role that river ice dynamics undertake in shaping river recession patterns. The existing discourse is yet to converge on a consensus regarding whether river ice dynamics serve as a barrier or possess a distinctive influence on delineating accurate river recession patterns.

Rive ice in a small alpine stream: A notable under representation exists in the study of river ice dynamics in smaller rivers despite their inherent large variability and rapid responsiveness to fluctuating processes (Turcotte and Morse, 2013; K. Alfredsen, Stickler, and Pennell, 2006; Buffin-Bélanger, Bergeron, and J. Dubé, 2013). These water bodies manifest significant variations in morphology and flow regimes within compact spatial boundaries, exhibiting diverse shapes and characteristics. The reduced water volumes traversing these rivers accentuate their sensitivity, making them more susceptible to a range of freezing processes that warrant meticulous scrutiny (Lind et al., 2016; Buffin-Bélanger, Bergeron, and J. Dubé, 2013). The geographic distribution of research efforts reveals another gap. Predominantly, investigations surrounding river ice formations are centralized in countries like Norway, Canada, and Japan, conspicuously excluding regions such as the Swiss Alps from the study's purview.

The magnitude of water retention due to river ice formation: A conspicuous gap remains in exploring the magnitude of water accumulation attributable to river ice formations, particularly in an alpine stream. This underlines the pressing need and relevance of the present study, aiming to foster more profound insights and comprehension of these phenomena.

1.3 Research questions

The research mentioned above gaps lead to the following research question, which is brought into the context of the case study of an alpine stream, the Dischmàbach. The low-flow of the Dischmàbach in winter is fed by various slow sources such as spring water or small lakes in the catchment. The flow of the Dischmàbach is called *dormant* because it is not responsive to large changes in winter (Schaefli, Rinaldo, and Botter, 2013). However, upon closer observation of the Dischmàbach's winter flow, notable fluctuations and irregularities in its hydrograph become apparent (*cfr. doctoral thesis of Michael Margreth*). These variations position the Dischmàbach as a valuable case for in-depth study, an ideal tool to address the following research questions.

- **RQ:** *How does ice formation influence the patterns and characteristics of winter discharge behavior in the Dischmàbach?*

Further detail, the question can be supplemented by the following two subquestions:

- **RQ1.1:** *Where along the course of the Dischmàbach does ice formation predominantly occur?*
- **RQ1.2:** *Can the water volumes retained by these ice formations be quantified?*

1.4 Thesis procedure

This thesis focuses on an exploratory analysis of ice formation in the Dischmàbach and discharge behavior over the cold season between 2022 and 2023, complementing Michael Margreth's doctoral thesis. The field study was conducted from November 2022 to March 2023. Thus, the water level was monitored at three measuring points in the river using pressure sensors, and wildlife cameras were used to take pictures. Water temperatures were also measured. Aerial drone imagery was used to capture specific periods of icing and map the location where ice was building up. In this study, a trial-pronged methodological framework was employed. First, a descriptive analysis centered on river morphology was undertaken, quantifying river attributes and leveraging systematic observations and digital terrain models (DSMs) to evaluate ice formation locations. Much of the data is visual, sourced independently from Swisstopo, and supplemented by water temperature measurements. The second strategy involves the design of a semi-automatic algorithm to analyze ice-retention volume. This tool processes runoff graphs to detect ice formations and gives a first estimate of the associated reservoir volumes caused by ice damming. The primary datasets used are from the Kriegsmatten gauging station and recent water level recordings enriched by imagery from wildlife cameras. A concise third approach involved analyzing water levels through drone imagery, comparing ice-rich to ice-free days. This allowed calculating water volumes retained due to ice during a single event.

Chapter 2

Study Site

The Dischmàbach is located in the Dischma valley near Davos, in the canton of Graubünden in Switzerland. The stream winds down in the valley's center until it joins the Landwasser River at Davos Dorf. It is one of the primary source streams for the Rhine catchment (schweizerfluss.ch, 2023). The primary underground water spring is beneath the Scalettahorn at approximately 3000 m a.s.l.(schweizerfluss.ch, 2023). Additionally, the Dischmàbach receives water from smaller tributaries and lakes in the side valleys (Swisstopo, 2023a). The catchment covers an area of 53.7 km^2 and extends from an altitude of 1545 m a.s.l. to the mountain peaks of Piz Grailesch and Scalettahorn at an altitude of 3180 m a.s.l.[3] The average slope is 26 °, where the main stream course is relatively flat (0-5 °) while the valley's side walls have an average steepness of 40 °. The primary orientation of the valley, or the stream flowing direction, is northeast. The lower parts of the valley are mainly covered with a coniferous forest (about 9 %), while the higher area is characterized by grassy and herbaceous vegetation (32 %) and wetlands (9 %). The steep slopes of the mountain flanks are mainly covered with rocks and unconsolidated stones. The Scaletta glacier covers 1 %[4] of the catchment (HADES, 2023). The main geological features are gneisses from the Silvretta cover and massive moraines deposited from the glaciers. More recently, the valley was shaped by mass movements and fluvial processes; the lower center of the valley is alluvial (FOEN, 2023).

[3]Starting from the confluence location into the Landwasser river.
[4]Considering the catchment area of ca. 42.9 km^2 from the FOEN measuring location in Kriegsmatten, Davos.

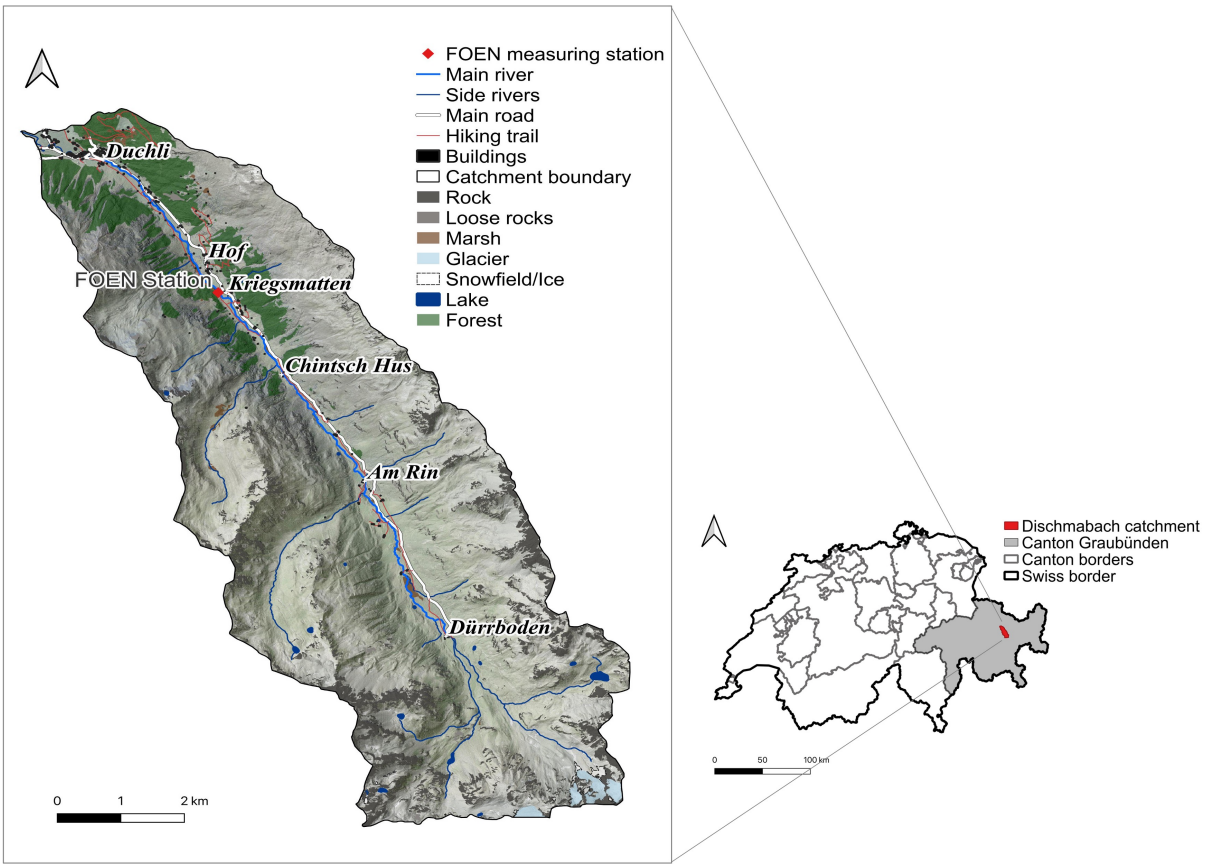

Figure 2.1: Overview map of the Dischmàbach catchment created in QGIS with the geodata from Swisstopo

Hydrological parameters: The climate of the study area is alpine, and the hydrological regime type is glacial-naval. The mean annual precipitation sum of the catchment is 985 mm, the mean air temperature is 0.6 °C, and the mean yearly discharge is 1.4 m^3/s (822 mm) (FOEN, 2023; HADES, 2023). In winter, between November and March, the mean precipitation is about 317 mm, the mean air temperature is -5.4 °C and the mean discharge decreases to 0.6 m^3/s (352 mm) (FOEN, 2023; HADES, 2023). The meteorological data is measured at the FOEN station in Kriegsmatten at 1600 m a.s.l (FOEN, 2023). Approximately in the middle of the valley (Figure 2.1).

Historical background: Since the 13th century, when the first settlements appeared in the valley, the alpine stream dictated the positioning of the buildings, and the stream's course was constantly changing and threatened to become a marsh. Therefore, in the early 1930s, 700 m of the stream was regulated (between Duchli and Hof, Figure 2.1). The controlled area remained wet because of the side streams and the clay-rich soil. To bring back the stream's natural function, this stream's stretch was revitalized in 2019-2020 (Davos, 2020). Today, few buildings are spread along the main road, of which only a part is inhabited all year round. There are no large agricultural areas. However, part of the meadows are used as pastures for cows in the summer.

Chapter 3

Data

In this chapter, the primary data used, which were essential for the realization of this work, will be discussed in detail. The data collection was done in two ways:

1. **Fieldwork-data**: Own data collection during field measurements in the Dischma Valley in winter 2022-2023. This data provides an up-to-date and direct insight into the studied area's current hydrological and climatic conditions.
2. **FOEN-data**: Existing data from official measuring station in Kriegsmatten (Dischma Valley), collected from 2004 to 2023 from the Federal Office for Environment (FOEN). This data forms a solid basis, as they were collected over a more extended period and thus provide a historical perspective.

3.1 Fieldwork-data

3.1.1 Measured Variables

Table 3.1: Collected data during fieldwork in winter 2022-2023*

	Unit	Sensor/Device	Recording interval
Pictures	-	Wildlife camera	15 min
Ortho images	-	Drone	5 times over the winter
Digital surface imagery (DSM)	-	Drone	5 times over the winter
Water temperature	°C	Temperature logger	5 min
Water level	m	Decentlab stage sensor	10 min
Water temperature	°C	Decentlab stage sensor	10 min

*Note: It should be noted that some problems occurred during the measurement campaign. Therefore the sensors did not record anything temporarily due to malfunctioning or some measurements were limited due to time restrictions.

3.1.2 Sensor/Device Placement

In the winter of 2022-2023, we conducted a field research campaign at the Dischmàbach in Davos to study ice formations in the stream. Initially, we conducted a comprehensive survey in October 2022, laying the groundwork by providing a thorough overview of the stream and its catchment. Guided by literature on ice formation in mountain streams and with insights from locals who witness these icy transformations every winter, we zeroed strategic locations for sensor placements (Figure 3.1). Notably, valuable input came from a retired gamekeeper, who pinpointed prime locations for our study (Frankhauser, 2022b).

The locations of the devices and sensors detailed in Table 3.1 can be seen on the map shown in Figure 3.1.

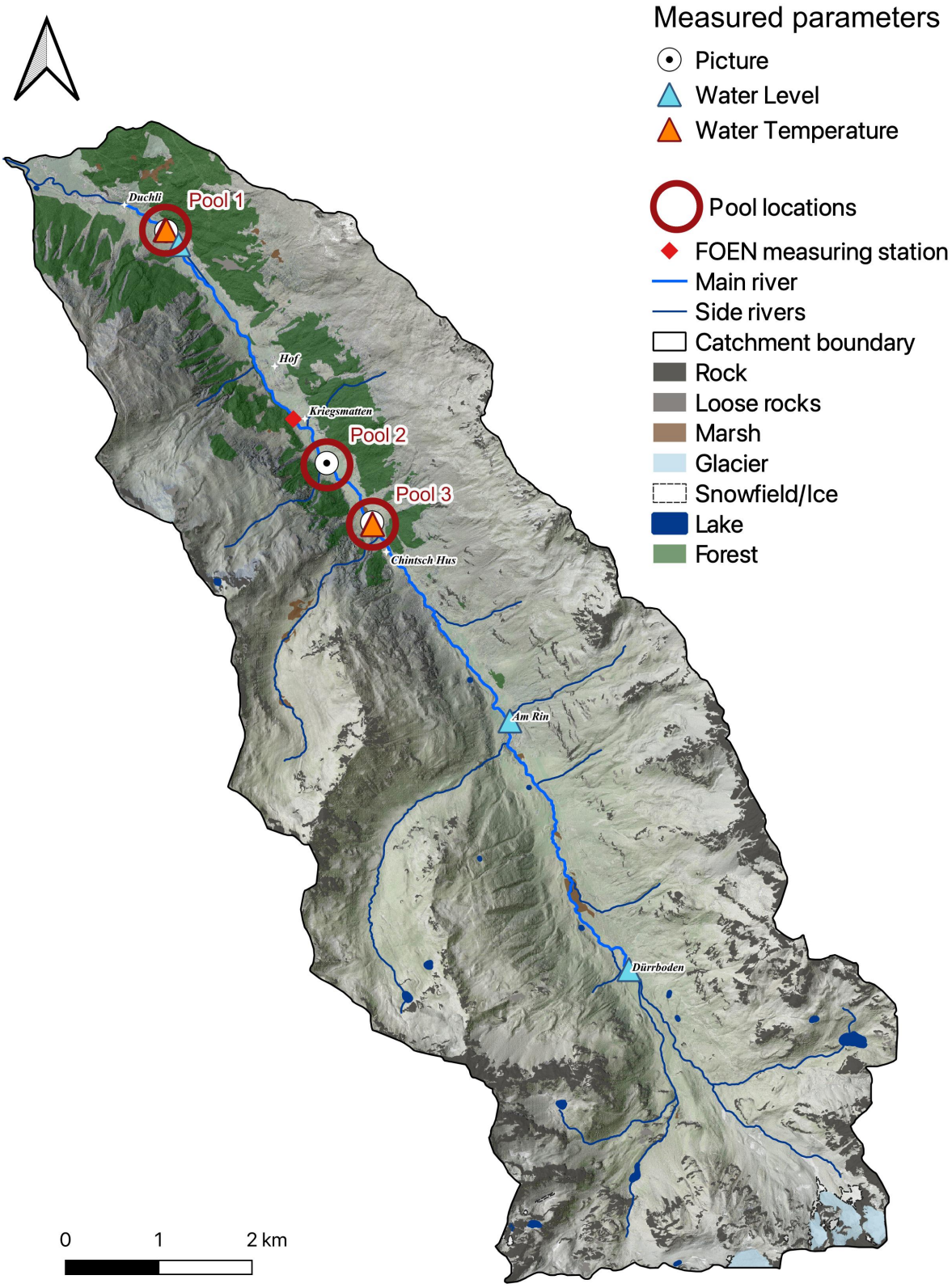

Figure 3.1: Overview map of the Dischmàbach catchment created in QGIS, with the placement of the sensors and devices during the field campaign of the winter 2022-2023

Three wildlife cameras were set up to capture real-time visual data at spots anticipated to accumulate ice, leading to pool formations 1-3. In line with the camera locations, four water temperature loggers were strategically installed to gauge temperature variations (Pools 1 and 3). Drone reconnaissance was employed over the stream, enabling us to pinpoint icy sections and gauge backwater occurrences. Water level sensors were systematically placed along the stream's course — at the start, middle, and end. Detailed information about the installed devices and sensors follows in the next sections.

3.1.2.1 Wildlife cameras

Three Bushnell Trophy Cam HD wildlife cameras, model number 119676 [5], were mounted on the streambank on wooden posts or adjacent trees (Figure 3.2). They were oriented to view stream sections where ice formation and an associated water level rise were expected to form. The cameras were configured to take a picture of the stream section in question every 15 min from 6:30 in the morning to 17:00 in the evening, under favorable lighting conditions. The captured images were stored on SD cards. The SD cards were replaced or read out with the batteries every 2 to 3 weeks.

Figure 3.2: Wildlife camera installed at Pool 1 (left), Pool 2 (middle) and Pool 3(right), pictures taken by Nina Nagel, 12.12.2022

- The camera at Pool 1 was installed on 09.11.2022 and presented the most complete data set with two data gaps between 20.12.2022 and 14.01.2023 and between 20.01.2023 and 06.02.2023.
- The camera at Pool 2, installed on 09.11.2022, presented data gaps between 16.12.2022 and 17.02.2023.
- The camera at Pool 3, also installed on 09.11.2022, had the most incomplete data set with a significant data gap between 10.12.2022 and 19.02.2023.

All three cameras were dismantled on 06.04.2023. Data interpretation should take these time constraints into account.

[5]The cameras were provided by Christian Rickli, a scientific staff member of the Mass Movement Group of the Swiss Federal Institute for Forest, Snow and Landscape Research (WSL).

3.1.2.2 Water temperature loggers

Four Vemco Minilog II-T Temperature Data Loggers[6], were used to record water temperatures. They recorded at 5 min intervals with an accuracy of 0.1 °C. The loggers were positioned upstream and immediately downstream of each morphological stream step to determine the temperature differences between the basin and the supposed ice-forming zones. Due to the limited availability of only four devices, the installation was at Pools 1 and 3 (see Figure 3.3 and Figure 3.4 for exact locations).

Figure 3.3: Location of T-Logger 1 and T-Logger 2 in Pool 1, pictures taken by Nina Nagel, 30.11.2022

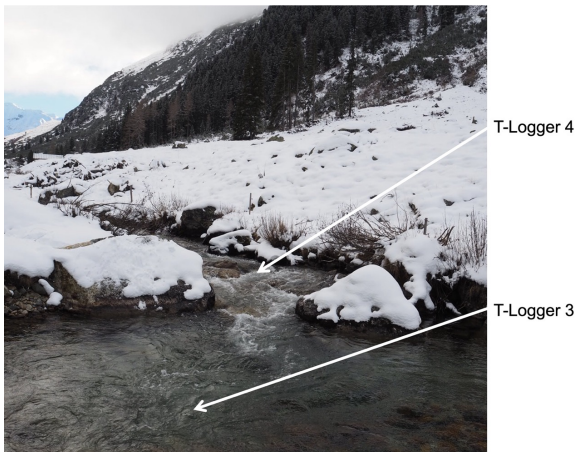

Figure 3.4: Location of T-Logger 3 and T-Logger 4 in Pool 3, pictures taken by Nina Nagel, 30.11.2022

Loggers were attached to heavy rocks or weights to secure them and lowered into the stream. To prevent them from washing away, they were also secured to a rock on the bank with a steel wire. This kept them only a few inches above the stream bottom. The loggers were installed on 30.11.2022, and they were removed on 06.04.2023. Data analysis was performed by M. Plüss. Temperature logger no. 4 did not show any measurement results due to malfunctioning.

3.1.2.3 Drone flights

Drone flights were carried out to map the icing locations in the entire catchment area and obtain a comprehensive overview. For this purpose, the drone *WingtraOne GEN II* was combined with the camera *Sony RX1R II* (wingtra, 2023b; wingtra, 2023a). During these flights, orthophotos with a spatial resolution of 2 to 3 cm and digital surface models (DSMs) with a resolution of 10 cm were generated. It should be noted that no control points were used during data collection. This results in potential deviations of the generated images of up to 10 cm in the x-y plane and up to 15 cm in the z-axis under snow conditions, which has to be considered in the results (Eberhard et al., 2021). A total of five drone flights were conducted[7]. The first flight was

[6]The loggers were provided by Michel Plüss, Technician in the group Aquatic Physics, EAWAG.

[7]To obtain a comprehensive overview of the entire catchment area, both with and without ice formations in the stream, eight flights would have been necessary. However, due to organizational and time constraints, only five flights could be conducted.

on 12.12.2022 and mapped the stream surface at the valley's upper end, between Am Rin and Dürrboden (Figure 3.5). At this time, ice formation in the stream was progressing. The second and third flight was conducted on 09.02.2023 and mapped the valley's two lower quarter, between Duchli and Hof, and between Hof and Chintsch Hus under freezing conditions. On 20.02.2023, 12 days later, two flights more were made of the two lower quarters of the stream, but under milder conditions with no stream ice formation (Figure 3.5). The drone flights were executed by specialists Yves Bühler and Andreas Stoffel from the Institute of Snow and Avalanche Research (SLF). They not only conducted the flights but also processed the imagery.

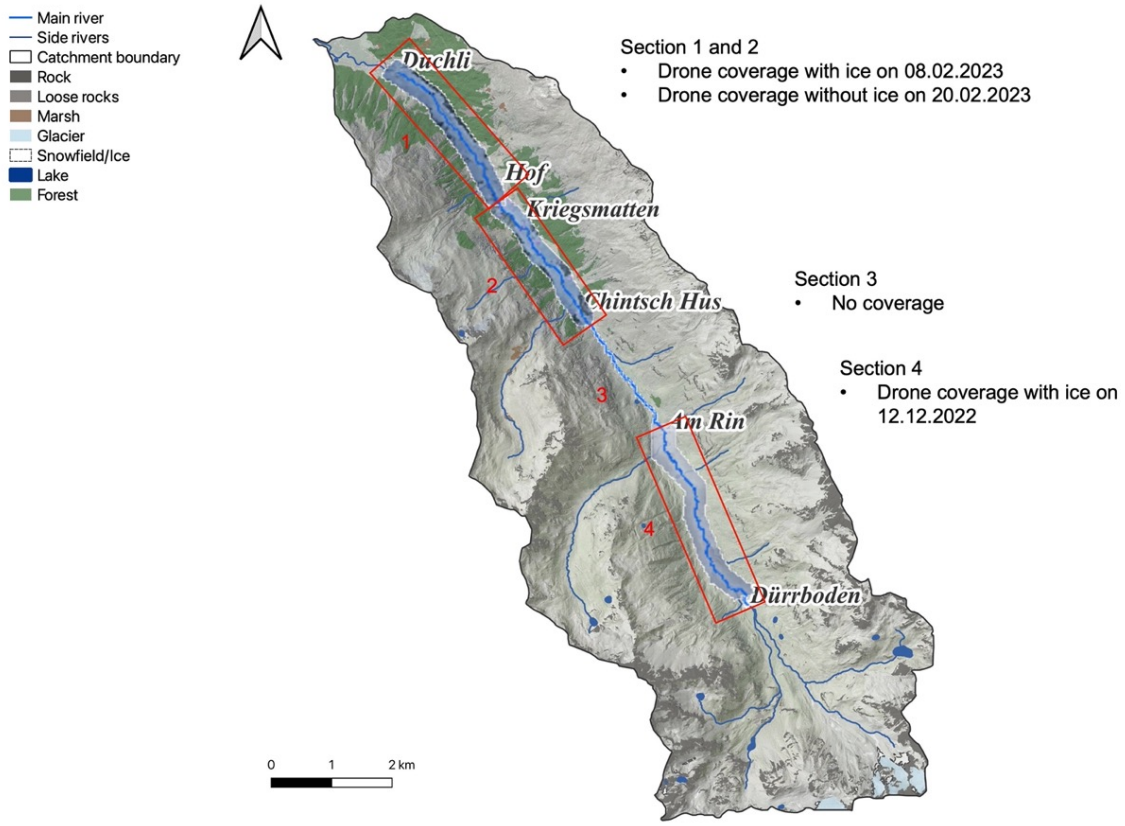

Figure 3.5: Map overview with the covered areas by the drone flights

3.1.2.4 Water-stage and water temperature sensors

Three *Decentlab DL-PR26* pressure and temperature sensors were installed in the stream for monitoring purposes [8]. They were positioned at the catchment's upper, middle, and lower ends at different bridges, respectively (see Figure 3.6). These sensors record the pressure of the overlying water column, from which the water level can be calculated, as well as the water temperature, at 10 min intervals.

[8]The loggers were provided by Dr. Jana Von Freyberg, Visiting scientist in the Mountain Hydrology and Mass Movements, Hydrological Forecasts Department at the Swiss Federal Institute for Forest, Snow and Landscape Research (WSL).

The conversion of the measured pressure into the corresponding water level follows the specific relationship:

$$\text{height} = \frac{\text{pressure [bar]} \times 100'000}{98.0665 \times 100} \tag{3.1}$$

The pressure measurement is in bar and has an accuracy of ±0.5 %. Water temperature is measured in °C with a resolution of 0.003 °C and an accuracy of ±2 °C (Decentlab, 2018). Sensor No. 2 and No. 3 were commissioned on 09.11.2022, while sensor No. 1 followed only on 07.02.2023. All sensors were uninstalled again on 06.04.2023.

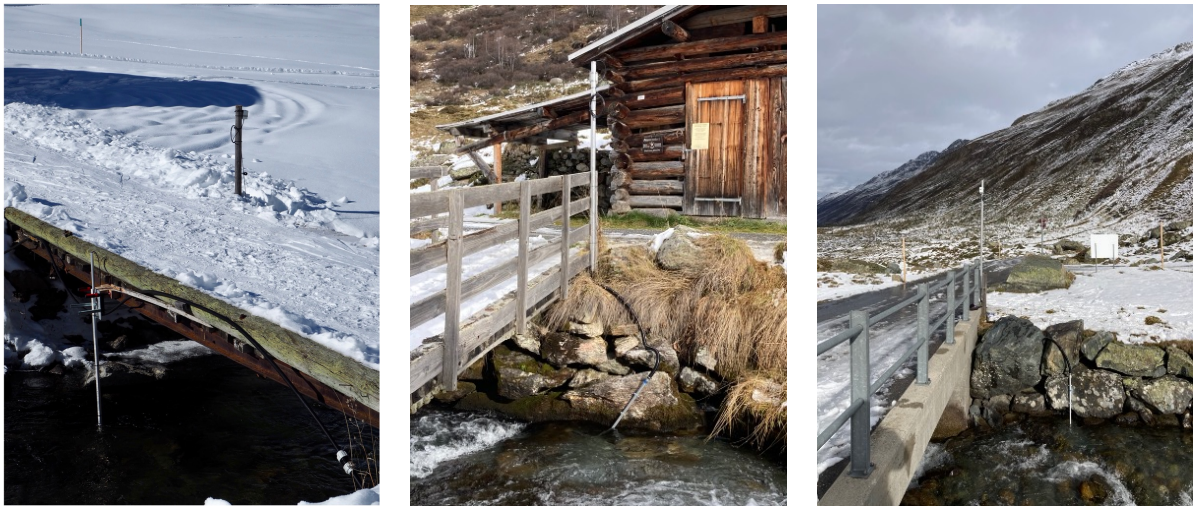

Figure 3.6: Stage sensor nr. 6166 installed near Pool 1 (left), nr. 6300 near Am Rin (middle) and nr. 12443 near Dürrboden (right), pictures taken by Nina Nagel, 09.11.2022 and 07.02.2023

3.2 FOEN-Data

In addition to the data collected independently, measurements by the Federal Office for the Environment (FOEN) at the Kriegsmatten station in the Dischma Valley were also used, covering the period from 2004 to the end of March 2023. The data collected include the following parameters:

- air temperature, recorded at 10-min intervals and given in °C
- water temperature, also recorded in 10-min intervals, in °C
- runoff rate, recorded at 10-min intervals and given in cubic meters per second (m^3/s)
- precipitation rate, determined as daily totals in millimeters (mm)

These data were requested from the hydrological department of the FOEN. It should be noted that the data from 2004 to 2022 have already been reviewed and cleaned for possible artifacts and other data errors by the appropriate authorities. However, the data for the period from 2022 to 2023 have not yet gone through this process.

In addition, geodata from Swisstopo were used, which include the following:

- Orthoimage, 25 cm, 2020, *Swissimage*
- Digital Terrain Model, 0.5 m, 2019, *swissALTI3D*
- Topographic raster map, 1:100000, 2023, *National Map with Relief*
- Topographic vector map, 2023, *swissTLM3D*
- Boundaries, 2023, *swissBOUNDARIES3D*
- Catchment boundaries, 2019, *Sub-catchment* 40 km^2

These geospatial data provide the resource for spatial analysis and support the analysis of hydrologic data by providing a geographic context for the phenomena under study.

Chapter 4

Methods

In the present thesis, three methodological approaches were applied:

1. **Morphological analysis of stream ice formation dynamics:** Descriptive analysis focused on stream morphology in connection to ice location: This focused on quantifying various stream characteristics, including the width and slope of the stream in connection with the ice formation. Systematic observations were used to describe and compare occurring ice formations. Using digital terrain models (DEMs) also allowed accurate determination of water surface elevation and the stream width. For this method, visual data sources were collected independently or provided by Swisstopo, supplemented by water temperature sensors and drone imagery measurements to map the ice locations.

2. **Event[9] analysis:** Development of a semi-automatic algorithm for ice-retention volume analysis. This Event-Finding-Algorithm was designed to analyze anomalies in runoff graphs, detect potential ice formations, and calculate the reservoir volume caused by ice. The primary data sources for this approach are from the federally operated Kriegsmatte gauging station supported by image frequencies from wildlife cameras that served as an additional basis for the analysis.

3. **Event-specific analysis utilizing drone images:** This entails the image analysis of Digital Surface Models (DSMs) acquired during drone flights. Utilizing the observed raised water levels at pool locations, the area is delineated, facilitating an approximation of the retained volume during singular events in the winter season.

Together, these three approaches provide a comprehensive insight into the phenomena studied and allow a holistic assessment of the situation.

[9] An "event" is understood as the occurrence of ice in the stream during the winter, which is substantial enough to dam the water at certain points in the stream and which is then visible in the hydrograph. Events are then identified by their start date.

4.1 Morphological analysis of stream ice formation dynamics

The morphology of a stream can significantly influence whether or not ice forms in it (Turcotte and Morse, 2013). For this reason, an investigation of the morphology of the Dischmàbach was carried out. The first approach starts from a broader view, considering the morphology of the entire stream course. Various factors, such as the streambed slope, width, water flow velocity, or different parameters, such as the Strickler or Manning values, can describe the morphology of a stream channel. To simplify and target the analysis of this complex system, this study considers two main features: the width and the stream's slope. Although these parameters may seem basic and straightforward, they play an essential role in the dynamics of the stream (Turcotte and Morse, 2013). The available elevation maps and orthophotos provided by Swisstopo were used for this analysis (Swisstopo, 2023b). The aim was to examine the course of the stream width as well as the inclination of the stream. Furthermore, drone images taken during icy conditions allowed the mapping of icing locations along the stream course.

The second approach occurred on a more local scale, which considered a detailed view of three locations of interest. Within the scope of this investigation, Pool 1, Pool 2, and Pool 3, were described and analyzed in detail.

4.1.1 Morphological characterization of the Dischmàbach

As part of an extended morphological analysis, the entire stream course between Duchli and Dürrboden was focused on. For this more comprehensive investigation, orthophotos and digital terrain models (DEMs) were used and analyzed using QGIS software. As previously described, the investigation focused on the width and slope of the stream. For this purpose, the stream course was divided into 2-meter segments to record the course of the width as well as the slope along the streambed.

Initially, the stream course was manually digitalized along the stream banks using QGIS. The existing stream dataset from Swisstopo (Swisstopo, 2023b) served as a starting point from which the actual course of the stream was extrapolated. More recent orthophotos from Swisstopo (Swisstopo, 2023b) and data from recent drone surveys were used to validate it and, if necessary, correct the determined course of the stream. A concrete example of the value of this verification is the inclusion of the correct course in the renaturation zone. This had not previously been mapped in the generally available datasets. The stream width and slope analysis combined QGIS and Python. Within QGIS, the stream course was first converted to a polygon. The central stream axis, or medial axis, was generated using the *HCMGIS* tool. This tool sporadically identified incorrect branches, which were corrected by smoothing and simplifying the line shapefiles. Python generated points and perpendicular lines along the medial axis at 2 m intervals. For each of these points, a line was created that was perpendicular to the corresponding section of the medial axis, allowing for a systematic and standardized method of determining

flow width at diverse locations (Appendix 9.1).

The stream width and the vector analysis tool *distance matrix* were calculated at the intersections between the stream banks. Each point along the medial axis was assigned a unique ID for systematization. The elevation along the stream was determined by assigning elevation values to the 2 m interval points along the medial axis. These values were based on a Swisstopo digital elevation model (DEM) with a resolution of 0.5 m (Swisstopo, 2023b) and were extracted using the raster analysis tool *sample raster values* in QGIS. The width and elevation data were then exported to the software R and could be aggregated there and further elaborated for the calculation of the slope and graphical representations.

Using the obtained drone imagery, the icing and water retention were identified manually along the stream course. Every point in a retention zone was assigned the value *1*, and every point in a no-icing zone was assigned the value *0*. Like this, an attribute table was exported and aggregated to the stream width and elevation information. Between every measurement point, the stream slope was then calculated with the following formula:

$$\text{slope} = \frac{z_i - z_{i-1}}{\Delta x} \tag{4.1}$$

Where:

- i is the point of measurement
- z_i is the elevation in m a.s.l. of i
- Δx is the distance between the measuring points, equal to 2 m

Visual scrutiny offered preliminary insights into trends and irregularities. In contrast, statistical parameter evaluation of the mean and standard deviation allowed a direct comparison between morphological characteristics connected to ice forming and morphological characteristics without ice forming.

4.1.2 Morphological characterization of the Pools

For the analysis of the stream morphology, Pool 1 and Pool 2 are first described on a small scale where ice formation was effectively observed. In addition, Pool 3 is described as a counterexample, where no ice formation was observed, nor was there any backwater. The description is based on images taken during the field visits, such as the interval images from the wildlife cameras and the morphology characteristics obtained from the geodata analysis. In addition, two pairs of temperature loggers have been installed at Pool 1 and one in Pool 3 (the fourth temperature logger did not record anything), which provide insight into the local water temperatures at freezing and non-freezing locations.

4.2 Event analysis

A semi-automatic algorithm for ice-retention volume analysis has been conceptualized and developed to advance our understanding and analysis of ice-related phenomena within aquatic environments (Event-Finding-Algorithm). This research method systematically identifies ice formation events and quantifies the respective backlog volume by analyzing the hydrograph trend.

The initial phase of this methodology entails the characterization of events documented by the wildlife cameras over the preceding winter season. This detailed characterization acts as a foundational reference point, or ground truth, upon which the algorithm is based. Following this, an algorithm was developed with a targeted objective: to accurately pinpoint and quantify occurrences of ice formation within the hydrograph.

As primary input, the data from 15.11.22 to 20.03.2023 was used, collected at the FOEN station in Kriegsmatten, and available in raw data format. In addition, the image recordings from the wildlife cameras between the 15.11.22 and 20.03.2023 at sites 1 to 3 were used to create a "ground truth", i.e., a reliable reference. In a further analysis phase, the FOEN stations' measured data from 2004 to 2022 were included in the algorithm. Within the period considered, both the coldest and warmest winters were identified, and in particular, the observed variations in these seasons were examined. In contrast to the more recent FOEN data, these historical data have been checked for errors to ensure accuracy.

4.2.1 Ground Truth: Event characterization

The events recorded by the cameras served as the basis for determining a ground truth. The recorded image sequence was subjected to a manual review. Three main criteria were used to identify significant ice formation: (1) The water level, which visually rises during the night and falls again at noon the following day; (2) the occurrence of ice formations, especially anchor ice; and (3) the roughness of the water surface, which during the retention gets very smooth and flat. Subsequently, the events were compared with the measured data from the FOEN station in Kriegsmatten, where air and water temperatures were recorded at different times (16:00, 24:00, 07:00, 12:00). This identified particular patterns that led to the division of the event analysis into two periods: "early" winter, which begins in early December and ends in mid/late February, and "late" winter, the period from mid/late February to end of March. The lowest temperatures are typically recorded in the morning at 7:00 $\pm$1 hour. Based on this observation, the water and air temperatures at 7:00 were used as reference values. It is assumed that during these minimum temperature conditions, the probability of ice occurrence in the stream is highest. In addition, the air and water temperatures of the events captured by the camera at that time were compared. The warmest temperature value was used as a reference, based on the hypothesis that at least this temperature is necessary to ensure sufficient ice formation in the stream to

cause waterlogging (Appendix 9.2).

Furthermore, it was observed that the freezing events only occurred on days without precipitation. Therefore, it was also assumed that accumulating ice would only form with a precipitation value of zero. Based on the above observations, thresholds were set, which will be used later in the event analysis. Due to the temporal distance, it is impossible to confirm the past's freezing events with certainty. Therefore, for the event analysis of the previous years (2004-2022), the study is based more on visual observations and assumptions supported by our own experience (Strohmenger et al., 2023). Given the annual climatic fluctuations, the search criteria were moderately adjusted. This analysis used search criteria corresponding to the "late" winter of 2022-2023.

4.2.2 Event extraction procedure

The analysis of icing events is divided into three methodological steps. In the first step, the freezing events are identified selectively by applying the criteria defined in Section 4.2.1 and evaluating the runoff graph course. In the second step, a fitting model for the data segment is used, which simulates the time course of the runoff, assuming that no ice is present in the stream. In particular, this model is intended to be representative of the stream's discharge recession behavior during the winter months (Tallaksen, 1995). In the third and final step, the No-Ice-Model determines intersection points with the discharge graph. These intersections then allow for precisely calculating various parameters and values related to freezing events.

4.2.2.1 Step 1: Event finding

To find the events in the data set, it was assumed that they only occur when the air temperature in the early morning is below the threshold and the water temperature is close to the freezing point. Furthermore, ice formation events only occur when there has been no precipitation. Another observation in the hydrograph is that the runoff gradient drops sharply during the ice formation events compared to the previous days. Therefore, the average of the runoff slope in the days before the event was compared with the average of the runoff slope during the event. An event is extracted only if the latter is steeper, i.e., more minor than the average runoff slope of the previous days. The time interval used to determine the slope of the pre-event discharge graph was tested with different interval sizes (Section 4.2.3).

4.2.2.2 Step 2: No-Ice-Model

To identify icing events and determine the amount of water backed up due to ice formation, it must be assumed that the discharge in an ice-free stage does not show any significant fluctuations. A discharge trend without ice was determined based on measured values, assuming that there is currently no ice in the stream and that the criteria of the first step are not met. Two approaches

were taken to analyze the icing events and the resulting runoff patterns. The first draws on the theory of runoff recessions, which states that runoff patterns tend to decrease exponentially (Tallaksen, 1995). The exponential trend was calculated for each case identified in Step 1. A fixed period before each event served as the basis for this calculation. The robustness was checked using different time intervals (Section 4.2.3). Consequently, the approach is based on local calculations for each event. The following equation was applied to

$$\hat{q} = e^{\beta_1 \times \mathrm{ID}} \times e^{\beta_0} \tag{4.2}$$

Where:

- $\hat{q}$ is the predicted discharge without icing events.
- β_1 is the coefficient for the predictor ID, i.e., `model$coefficients[2]`.
- β_0 is the intercept, i.e., `model$coefficients[1]`.

The second approach is, on the contrary, a statistical calculation. Moreover, this approach does not proceed locally but from the whole data set. Here, the discharge was calculated using *smooth.spline*. This function fits a cubic smoothing to the data, finding a trade-off between smoothing and goodness of fit. The goal is to visualize the course of the data by smoothing it (Eubank, 1999). A smoothing parameter between 0 and controls the trade-off ∞. With a parameter value of 0, no compromise is made between "goodness of fit" and smoothing, i.e., every data point is represented accurately. With increasing penalty parameters, on the other hand, the data set is increasingly smoothed. In this analysis, the smoothing parameter was set to 0.8, chosen through visual assessment of the best fit.

4.2.2.3 Step 3: Intersection Points

In the first step, the freezing events were identified punctually from the data set. In this last step, their duration is determined by the intersection points between the No-Ice-Model and the runoff diagram. The amount of impounded water during freezing can also be calculated: it corresponds to the area between the two lines. It is also possible to derive the average amount of impounded water throughout the event, the temporal length of such an event, and the proportion of water impounded by ice concerning the expected runoff according to the No-Ice-Model. To identify the intersection points between the No-Ice-Model and the discharge graph, a linear function was drawn between each measured point of discharge and each calculated point of the No-Ice-Model. This allowed the intersection points between these linear functions to be identified, considering only those that fell between the selected time points. Based on the assumption that during an icing event, the discharge initially decreases as water is impounded, and when the ice breaks up, the discharge increases again. First, the right and then the left intersection points in the graph could be extrapolated (Figure 4.1).

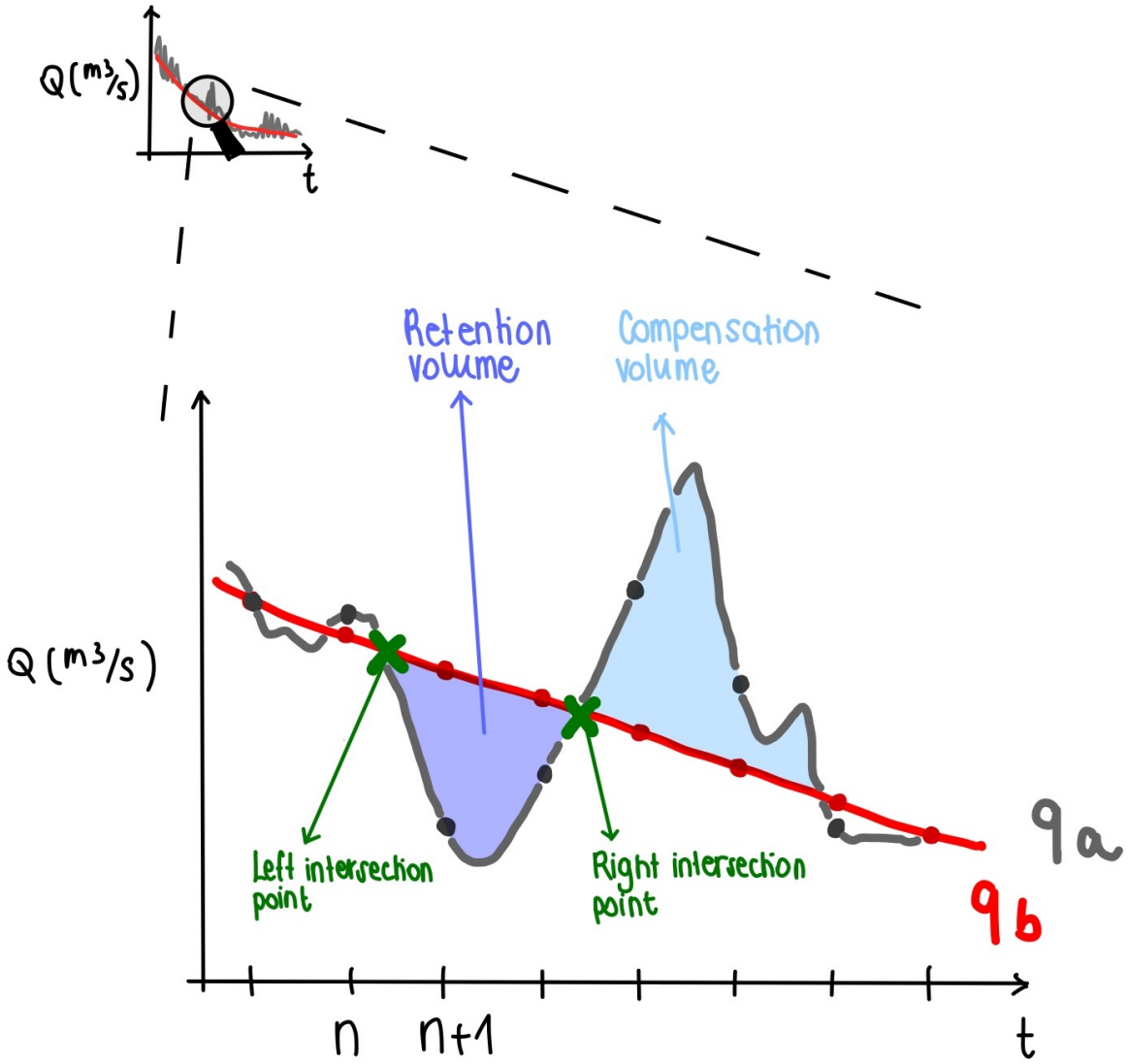

Figure 4.1: Sketch illustrating the step 3 procedure, drawn by Nina Nagel

The following equations were used to find the intersection points:

$$\begin{aligned} q_a(n) &= \frac{q(n+1) - q(n)}{ID(n+1) - ID(n)} \\ q_b(n) &= q(n) - q_a(n) \times ID(n) \\ m_a(n) &= \frac{m(n+1) - m(n)}{ID(n+1) - ID(n)} \\ m_b(n) &= m(n) - m_a(n) \times ID(n) \end{aligned} \tag{4.3}$$

Where:

- n is the point in time
- q_a is the stream discharge

- q_b is the expected discharge by the No-Ice-Model
- m_a is the slope of the linear function between n and $n+1$ for the stream discharge
- m_b is the slope of the linear function between n and $n+1$ for the expected discharge by the No-Ice-Model

4.2.2.4 Calculated parameters

As previously explained, the algorithm allows determining specific parameters for each recorded event. These parameters include the volume of water accumulated during the event and the duration of each respective event. Additionally, the water discharge, which is predicted according to the No-Ice-Model, can be calculated, enabling quantifying the proportion of accumulated water. In the study, the compensation volume was also determined. This term refers to the area on the hydrograph that lies between the line of the No-Ice-Model and the discharge line but is positioned above the No-Ice-Model (Figure 4.1. This area represents the release of the accumulated water. The determination of this volume could be realized using the "end-hour", i.e., the moment when the rising hydrograph intersects the No-Ice-Model until the next point of negative fluctuation.

The following parameters are obtained after the application of the algorithm:

- Retention Volume, the area below the discharge line, and the No-Ice-Model
- Retention time, duration of the event during which ice is retaining water
- Mean retained volume, the volume retained during the freezing divided by the duration of the event
- Expected discharge by the No-Ice-Model
- Percentage of retained mean volume in comparison to the expected No-Ice-Model
- Retention discharge, anticipated No-Ice-Model discharge minus the mean retained volume
- Compensation Volume: released volume of water after the freezing
- Compensation discharge, expected No-Ice-Model discharge, plus the compromise compensated volume
- Difference discharge between the compensation and retention discharges, showing the magnitude of an event

4.2.3 Model validation

The algorithm's robustness was tested by considering two crucial factors: first, by varying the pre-time and second, by using two different No-Ice-Models (Section 4.2.2.2). The pre-time was evaluated using tests with varying lead times of 3, 5, 7, 10, and 14 days. The resulting outputs were then correlated with observations captured by cameras to identify the best-performing model. This approach allowed for a nuanced evaluation of model performance and uncovered potential improvements and optimizations to the algorithm.

4.3 Event-specific analysis utilizing drone images

The procedure described here analyzes a single event made possible by subtracting drone aerial photographs. As part of this procedure, the stream was flown over at time points with icy and ice-free conditions. The resulting digital surface models (DSMs) were compared to identify the difference in Z-values to detect the change in water level. The flight mission with ice-rich conditions occurred on the morning of February 8, 2023, while the flight to record ice-free conditions was conducted on the morning of February 20, 2023, under comparable meteorological conditions. The flight area of those surveys extended from Duchli to Chintsch Hus (Figure 3.5). The identified differential grids were segmented into different Z-value categories to allow specific focus on the water surface. To ensure more efficient identification, the other elevation difference classes were color-coded. Detailed analysis of the elevation differences along the stream's course allowed for precise delineation of the extent of impoundment within the basin of interest. Subsequently, the areas of impoundment, categorized by the corresponding Z-value classes, were aggregated and multiplied by the respective Z-values to calculate the total impounded volume. In the third segment, from Am Rin to Dürrboden, potential dam areas were identified by analyzing ortho-images captured on December 12, 2022. Due to the lack of ice-free comparative data, the volume increase estimation for this segment is based on a rough approximation derived from ortho-image analysis, with an estimated water surface increase of about 45 cm. It should be noted that there was a data gap in the area between Chintshus and Am Rin (Figure 3.5), comprising about a quarter of the total stream surface area. A quarter of the determined volume from the other segments was added to the damming volume estimation calculations to account for this.

Chapter 5

Results

The following chapter will present the central results obtained using the methods outlined in Chapter 4. In addition to this, significant findings from the measurements, which serve as complementary information facilitating a more in-depth analysis, will be presented.

5.1 Morphological analysis of stream ice formation dynamics

5.1.1 Stream morphology

The analyzed section of the Dischmàbach extends 11.09 km from Duchli to Dürrboden (Figure 2.1). On average, it measures 5.88 m in width and has a downstream mean slope of 0.038[10]. Variations in width and slope were measured at intervals of 2 m, as depicted in Figure 5.1.

[10]The slope was calculated as depicted in Equation 4.1, and has thus no unit

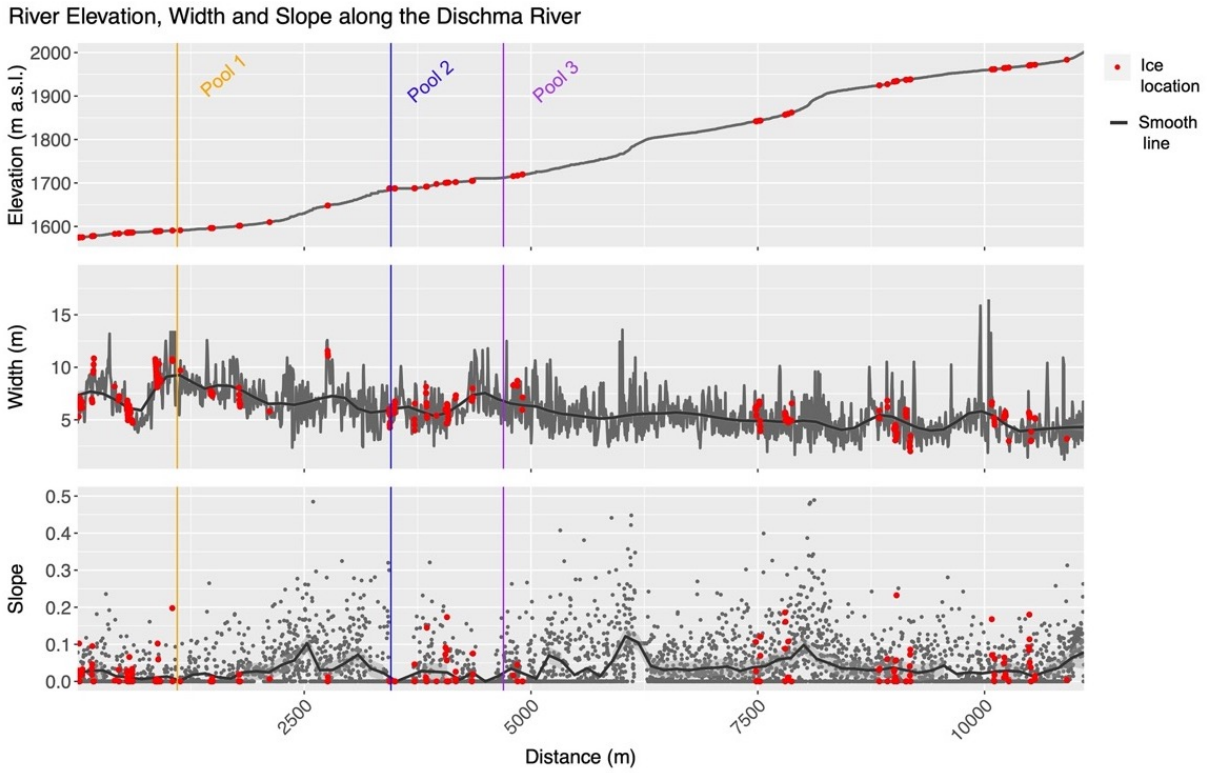

Figure 5.1: Elevation, width, and slope along the Dischmàbach measured/calculated for every 2 m and the locations showing a rise in the water level (red dots)

Figure 5.1 illustrates simple morphological features along the stream. The top graph shows the stream course at the altitude. The middle graph displays the stream width, supplemented by a smoothing line, and the bottom graph visualizes the slope with a point distribution and a smoothing line. The data reveals that the stream's slope and width vary greatly. The width ranges from narrow passages of about 2.5 m to expansive areas nearly 20 m wide. The slope fluctuates between 0 and approximately 0.5. Additionally, it has been noted that there is a progressive expansion in the stream's width, accompanied by a diminishing slope gradient as one approaches the valley region. The graph's red-marked points signify the locations identified as susceptible to ice damming, as delineated through aerial mapping conducted via drone flights. A significant section between km 5 and 7.4 shows no ice formation, which, however, is attributable to a missing drone flight and was, therefore, excluded from the analysis. In addition, the graph marks the positions of Pools 1, 2, and 3, which will be further investigated in subsequent chapters.

A brief statistical analysis scrutinizes the mean and standard deviation of the stream's slope and width characteristics. Within this study, the characteristics of regions identified as "icy spots" (1) are contrasted with those termed "ice-free spots" (0), as delineated in Table 5.1. Stream slope and width at the location where ice built up result in flatter and broader than the ice-free spots.

Table 5.1: Statistical parameters evaluating the stream morphology

Ice	Mean slope	Sd slope	Mean width	Sd width
0	0.039	0.084	5.86	1.99
1	0.0253	0.059	6.42	1.91

5.1.2 Pool morphology

5.1.2.1 Pool 1

The Pool 1 study area is located at the lower end of the catchment, right away downstream of the renaturalized stream segment. This stream segment is close to a meadow, where the cross-country skiing trail is located in winter. Near the stream, the vegetation is characterized by a mixture of individual young conifers and a dominant older conifer, where the wildlife camera was positioned. Adjacent grasslands, pushed into the stream by weight and snow load, characterize the riparian area. The stream edges have stone deposits with an average diameter of about 50 cm, whereas, in the middle of the stream, the stones have a smaller diameter of about 5-10 cm. A distinct morphological step within the streambed is evident that creates a rapid for that area. More immense boulders characterize this stream stage. The step has a height of about 50 cm, and the stream has a 5.5 m width. Upstream of this stage, the stream flows smoothly without significant width variation. The slope of the streambed upstream of this stage is circa 0.089, and the mean width is 5.61 m. Several more steps are found downstream of the first morphological step, leading to a lively, bubbling section of the stream. At this point, the slope of the streambed is 0.10, and the mean width is 5.52 m. Figure 5.2 illustrates the morphology in 2 m measuring intervals. The red zone represents Pool 1, which shows water increase (red dots) just behind the mentioned step.

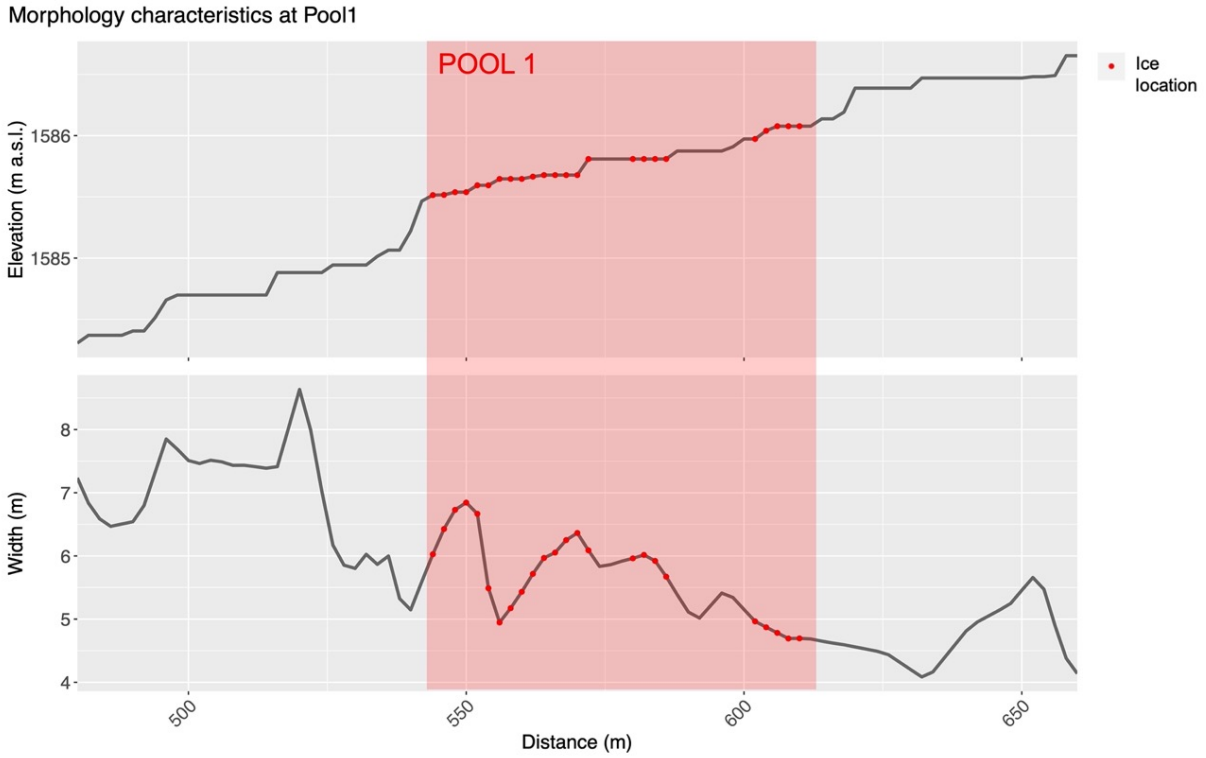

Figure 5.2: Stream elevation and stream width along the Dischmàbach every 2 m around the location of Pool 1 (red area) and the locations showing a rise in the water level (red dots)

During the first frost periods, anchor ice forms, specifically at the above-mentioned stage. This phenomenon has been observed in previous years by the local population of the valley, which also drew our attention to this area (Frankhauser, 2022a). One of the first documented ice formations occurred on 12.12.2022. Photographic documentation illustrates the formation of a layer of anchor ice and slush ice in the streambed. This ice acts against the natural stream flow and induces water retention (Figure 5.3). As winter progresses, after the first morphological stream stage, the emergence of a sheet of ice can be observed that extends across the entire width of the stream. While the water flows under this ice formation during the day (Figure 5.4), during cold nights, the combination of ice cover and growing anchor ice acts as an additional obstacle for the water, causing a significant damming effect (Figure 5.5).

Figure 5.3: Pool 1 the 12.12.2022 at 08:30 showing anchor ice formation and water retention, picture taken by Nina Nagel

Figure 5.4: Pool 1 the 07.02.2023 with the ice cover over the stream, picture taken by Nina Nagel

Figure 5.5: Pool 1 the 08.02.2023 during a freezing event and the ice cover over the stream, picture from the wildlife camera

Two temperature loggers were positioned in the Pool 1 area to record water temperature at different points in the pool throughout the winter. T-Logger 2 was placed at the top of the pool, while T-Logger 1 was placed closer to the morphological step, slightly further down (Figure 3.3). Figure 5.6 below illustrates the water temperatures in Pool 1 correlated to the icing events captured by the cameras. Noticeably, the water temperatures are close to 0 °C during icing events. This condition occurs over a more extended period for T-Logger 1, which is positioned directly at the ice formation stage. In contrast, T-Logger 2 usually shows increased water temperatures after such phases.

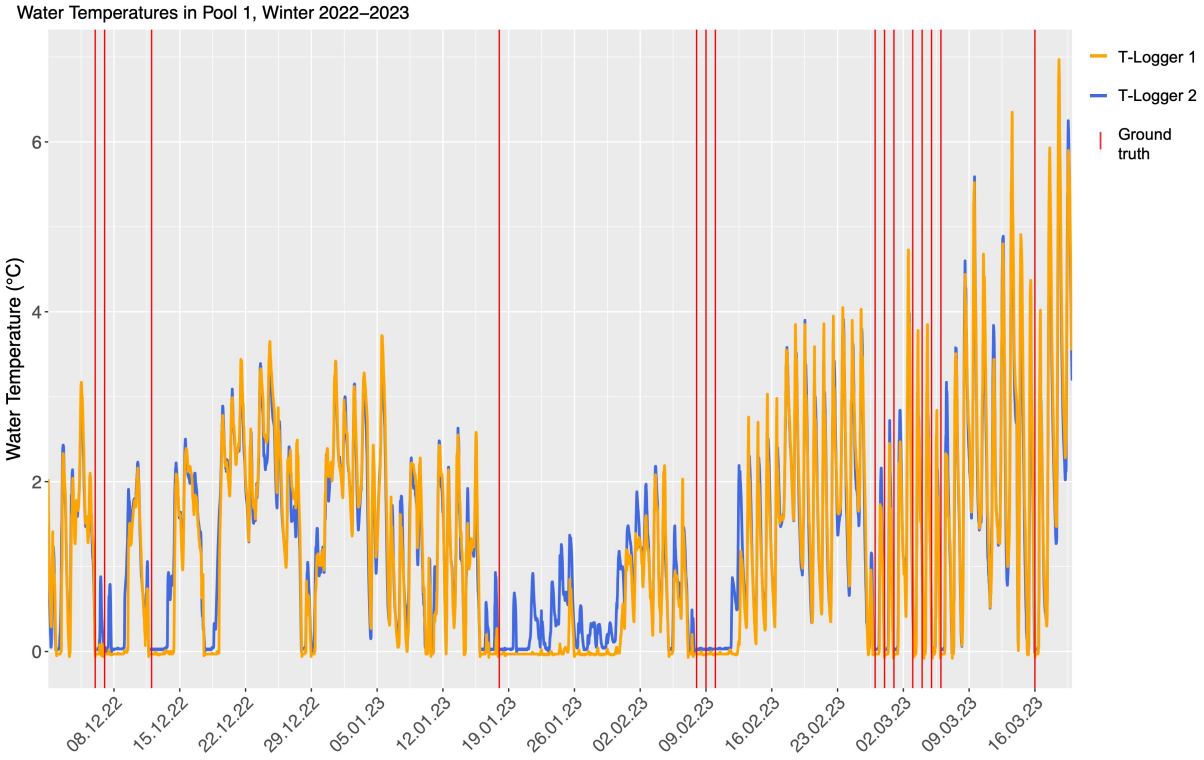

Figure 5.6: Water Temperature in Pool 1 between December 2022 and March 2023, one near the morphological step (T-Logger 1) and the second further behind the morphological step (T-Logger 2)

5.1.2.2 Pool 2

Pool 2 is centrally located in the catchment area and at the level of the Teufi restaurant, not far from a hiking trail. The vegetation in the surrounding area is characterized by grassland, various bushes, smaller deciduous trees, which are defoliated in winter, and isolated young conifers. Some of the shrubs extend to the banks of the flowing water. Upstream, the stream meanders between larger rocks before spreading out at the location of Pool 2. Following this, a morphological stage appears in the stream course dominated by rapids running between a mix of larger and smaller rocks. In the upper segment of the stream, the width measures approximately 4.3 m, and the slope of the streambed is 0.001. Where Pool 2 is located, the stream widens to a wider section with a reduced slope, the dimensions being 5.51 m wide and a slope of 0.039. Fewer large boulders are present in this section, and the water depth is relatively shallow. After this section, the slope of the stream increases and is 0.4, with a width of 5.8 m (Figure 5.7 and Figure 5.8). In Figure 5.7, the stream morphology illustrates an extended flat stretch, likely attributable to some inconsistencies in the DEM data rather than an accurate representation of the actual terrain. Despite this, a characteristic step morphology is discernible shortly downstream from the pool location.

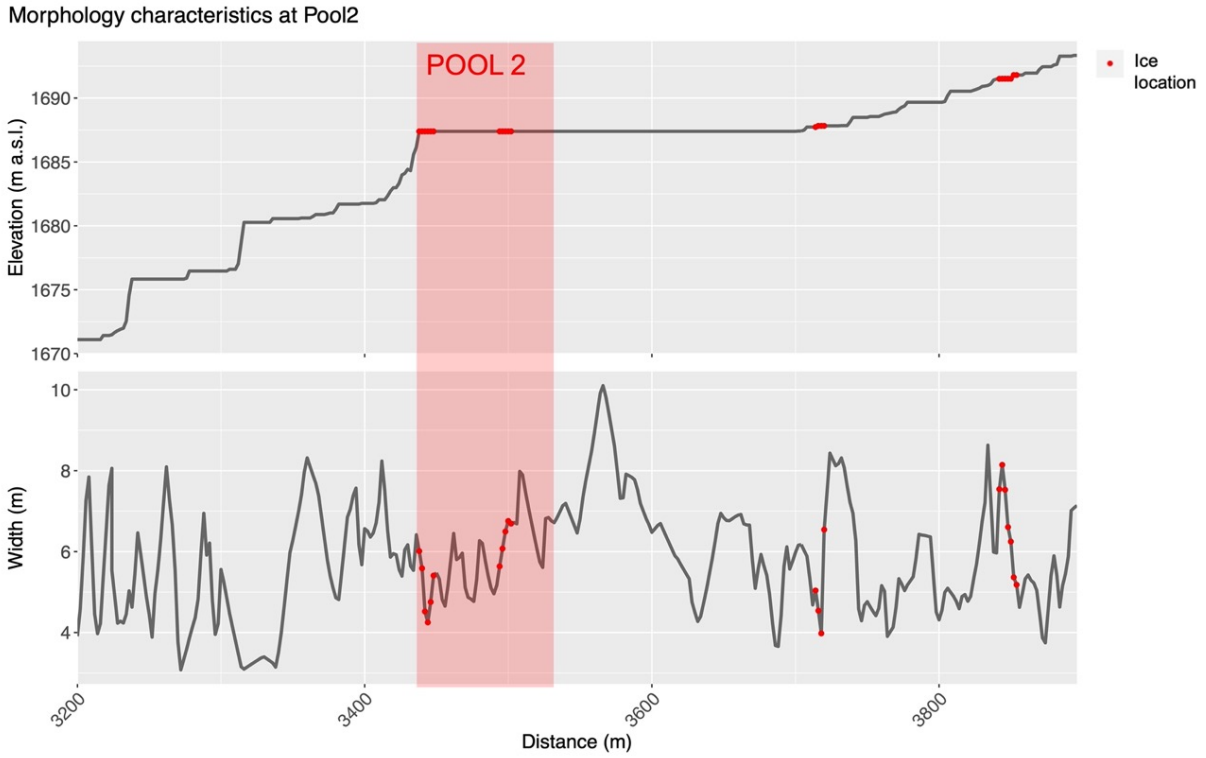

Figure 5.7: Stream elevation and stream width along the Dischmàbach every 2 m around the location of Pool 2 (red area) and the locations showing a rise in the water level (red dots)

During periods of frost, anchor ice forms between the stones of the downstream section, which inhibits the flow of water, causing a backwater and thus increasing the water level in Pool 2 (Figure 5.9).

Figure 5.8: Pool 2 on the 21.03.2023 with no anchor ice formation and water retention, picture from the wildlife camera

Figure 5.9: Pool 2 on the 08.02.2023 with retention due to ice formation, picture from the wildlife camera

5.1.2.3 Pool 3

Pool 3 is located farthest up in the watershed than the other pools and is situated between the road and the hiking trail. Meadows and shrubs dominate the surrounding vegetation; bigger

trees are not found in the immediate area. The morphological characteristics of this section of the stream include a course that flows over several steps in the upper segment and finally flows between two massive boulders with a diameter of about 2 to 3 m through a small waterfall into a spacious basin. Subsequently, the stream runs in a regular pattern. This pool is characterized in particular by the dimensions of the basin, which differs from the other places described in its width and depth. The nearby waterfall has a height of about 75 cm. In the upper segment of the stream, the width is 6.55 m, and the slope is 0.04. The basin measures 12.5 m in width with a slope of almost 0, while the lower segment has a width of 6.06 m and a slope of 0.03 (Figure 5.10).

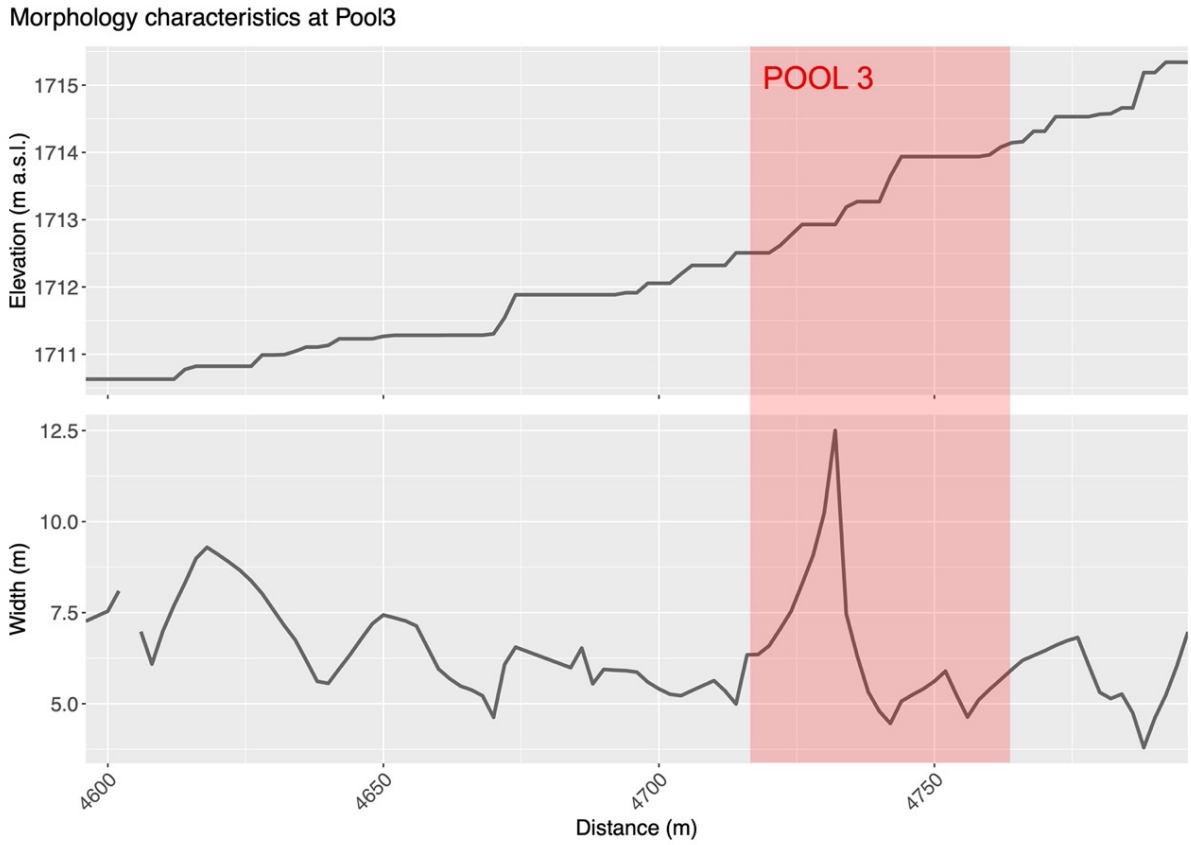

Figure 5.10: Stream elevation and stream width along the Dischmàbach every 2 m around the location of Pool 3 (red area)

Despite periods of frost, no ice formation was observed in this section. The stream ran constantly without accumulation. Anchor and slush ice formation were only observed at the basin's edge but did not extend across the entire stream width. Figure 5.11 captured on December 12, 2022, illustrates a notable discrepancy in ice formation patterns: while other pools and stream sections displayed significant ice accumulation, Pool 3 remained devoid of any ice formations. This was repeated on February 08, 2023, where significant ice formation was observed in Pool 1 and 2 but nothing in Pool 3 (Figure 5.12).

Figure 5.11: Pool 3 on the 12.12.2022 not showing any ice formation that causes water retention, picture taken by Nina Nagel

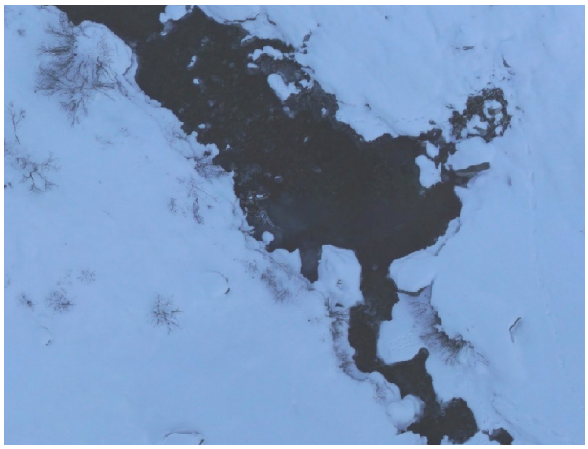

Figure 5.12: Pool 3 the 08.02.2023 with no visible ice formations, screenshot from the drone flight ortho image

Water temperature loggers were also installed in the area of Pool 3 (Figure 3.4). Unfortunately, T-Logger 4 was not functional. The measurement data from T-Logger 3 are shown in Figure 5.13 below. It can be seen that the water temperature does not drop to 0 °C during the majority of the freezing events recorded by the camera. Only during the events on 06.12.2022, 07.12.2022, and 12.12.2022 do the water temperatures approach freezing.

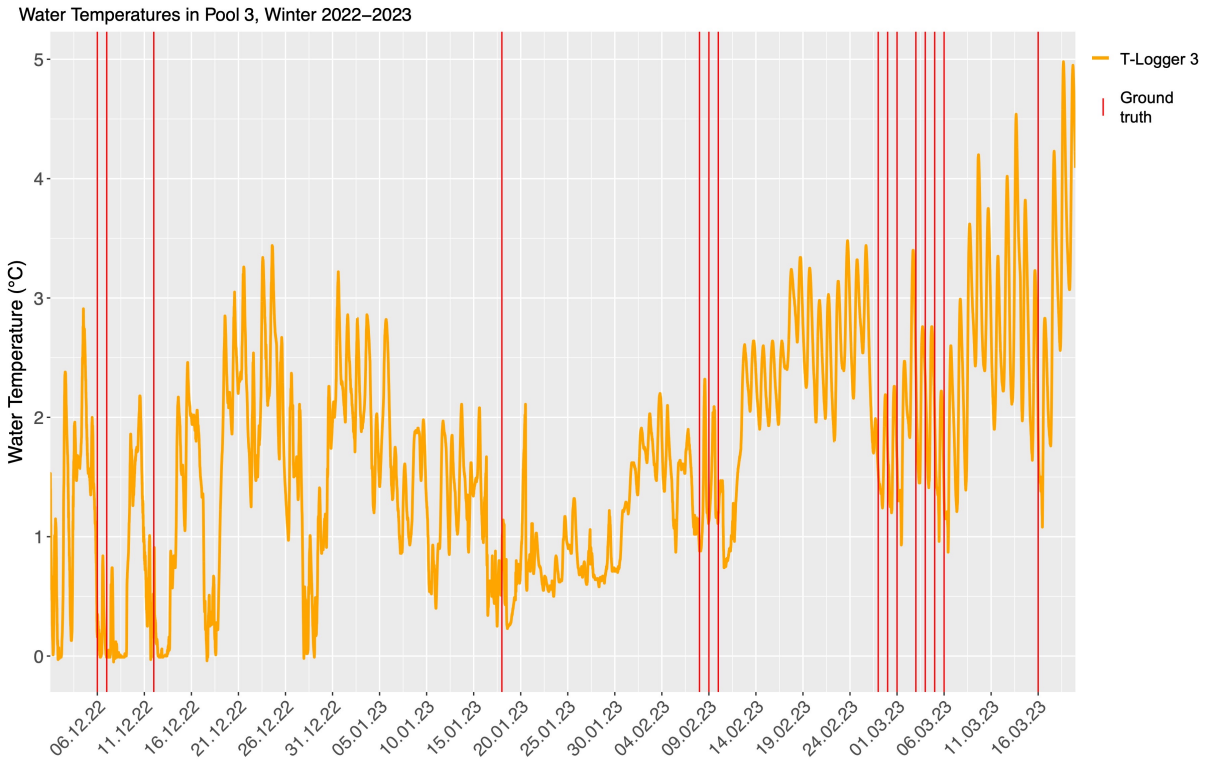

Figure 5.13: Water temperature in Pool 3 between December 2022 and March 2023

5.2 Event analysis

5.2.1 Event characterization

A total of 15 ice formation occurrences were identified with the wildlife cameras in Pool 1 and 7 in Pool 2, the latter coinciding in time with Pool 1 (Appendix 9.2). No ice formation was identified in Pool 3. Subsequently, by correlating the observations with the data recorded at the FOEN station in Kriegsmatten, the following thresholds were established for the event extraction algorithm applied for the winter of 2022-2023:

Table 5.2: Threshold values

Parameter	**Threshold value early winter**	**Threshold value late winter**
Air Temperature (°C)	-8 ± 0.5	-6 ± 0.5
Water Temperature (°C)	0.15 ± 0.05	0.25 ± 0.05
Precipitation (mm)	0	0

5.2.2 Validation

The resilience of the event-finding algorithm was evaluated by using different pre-time values about the verified events. In this context, pre-time intervals of 3, 5, 7, 10, and 14 days were applied for the *smooth spline* and *exponential decay* No-Ice-Model. The evaluation focused on the total number of freezing events identified by the No-Ice-Model and the number of events confirmed by the wildlife camera. The tables below show the results:

Table 5.3: Total event count of the No-Ice-Models over the winter 2022-2023

Pre-time	***smooth spline***	***exp***
3 days	19	17
5 days	19	16
7 days	17	15
10 days	16	15
14 days	14	13

Table 5.4: Number of events detected by the No-Ice-Models matching the ground truth event count (tot. 15) over the Winter 2022-2023

pre-time	***smooth spline***	***exp***
3 days	13	12
5 days	13	12
7 days	10	10
10 days	10	10
14 days	8	7

Data analysis revealed that a pre-time interval of 5 days produced the most optimal results for both models as it obtained the highest number of found events in total and the highest number of events corresponding to the verified events by the wildlife camera pictures. As a next step, both models were visualized, and Figure 5.14 and 5.15 were subjected to a comparative analysis.

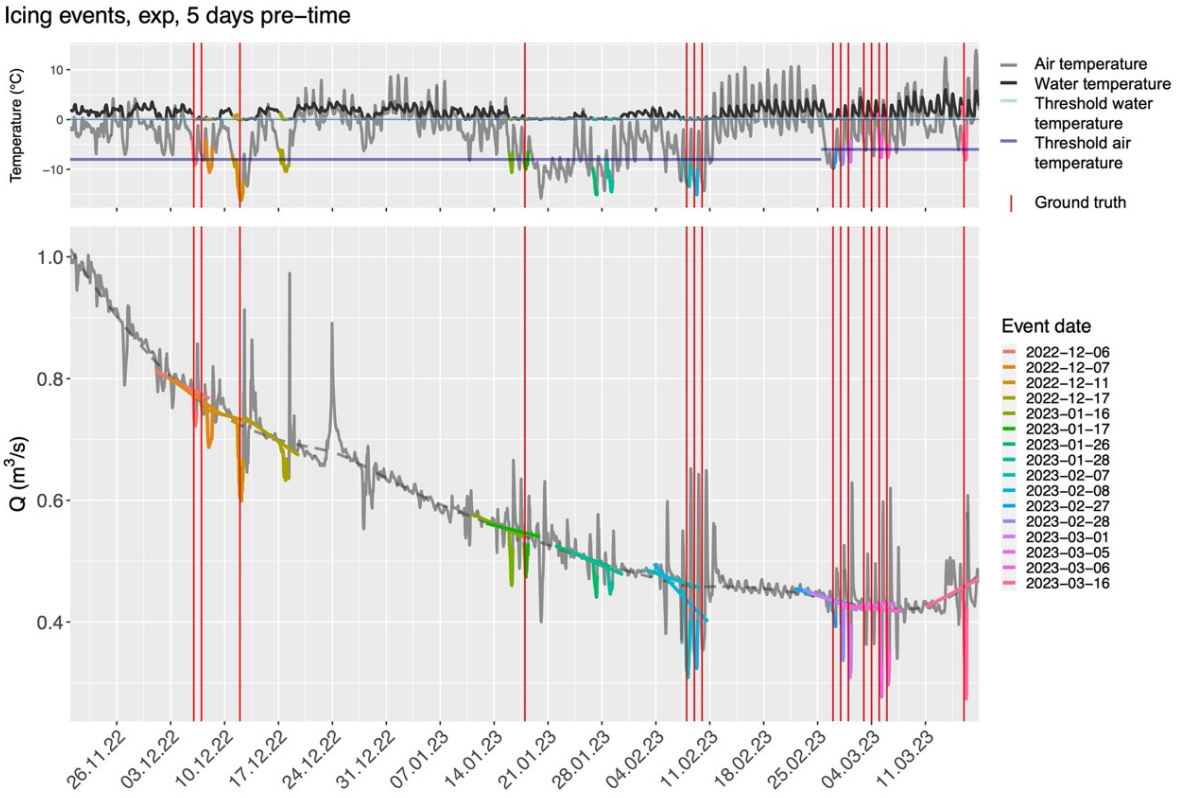

Figure 5.14: Overview of the found events by the algorithm with the *exponential decay* No-Ice-Model and a pre-time of 5 days with the events detected by the wildlife camera(red lines)

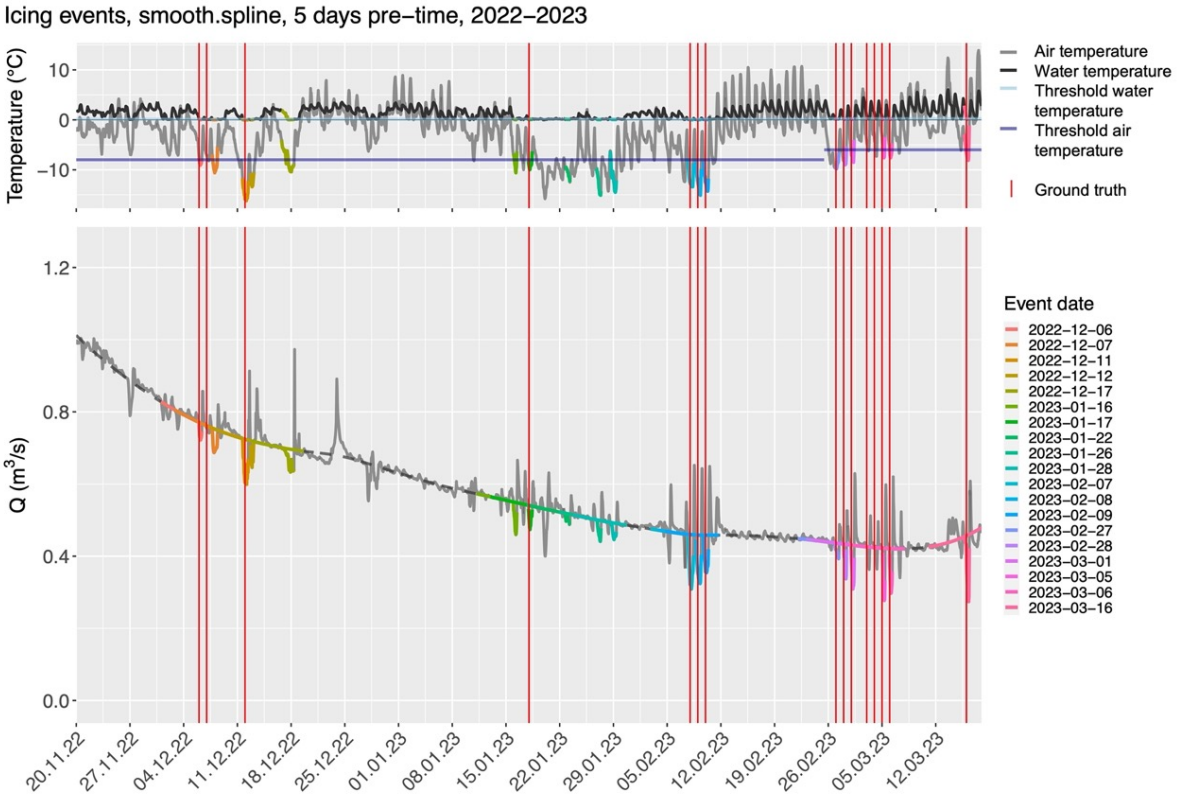

Figure 5.15: Overview of the found events by the algorithm with the *smooth spline* No-Ice-Model and a pre-time of 5 days the events detected by the wildlife camera(red lines)

Figures 5.14 and 5.15 illustrate in the upper graph the dynamics of air and water temperatures throughout the winter of 2022-2023 (from mid-November 2022 to mid-March 2023), as depicted in hourly averages, as well as the discharge recorded at similar intervals at the FOEN station in Kriegsmatten in the lower graph. The red vertical lines delineate the events identified through wildlife camera imagery, thus representing the ground truth data. The color-coded data segments indicate the events detected by the Event-Finding-Algorithm, with the lines corresponding to the color of the events representing the respective No-Ice-Model.

Figure 5.14 identifies events portrayed by the *exponential decay* No-Ice-Model. This model computes a no-ice discharge course locally for each found event and is characterized by the event's pre-time and length. It is observable that this model generally exhibits a visually coherent trajectory, albeit showing significant deviations around the events of February 7-8, 2023. Employing this approach, 16 events were identified, of which 12 coincide with the 15 verified events.

Contrarily, Figure 5.15 showcases the events identified through the *smooth spline* No-Ice-Model. Unlike the preceding approach, this model is predicated upon analyzing the entire winter data set. Therefore, the dashed gray line delineates the comprehensive *smooth spline* curve. The multicolored segments illustrate the events identified by the Event-Finding-Algorithm, accompanied by corresponding lines along the *smooth spline* curve. This approach unveiled 19 events, with 13 corroborating the verified events.

A comparison of the two models suggests that the *smooth spline* No-Ice-Model might be more aptly suited for finding the events and calculating the water volume accumulation during an icing, as it seems to represent the discharge trajectory most accurately.

5.2.3 Events and volume analysis results

5.2.3.1 Winter 2022-2023

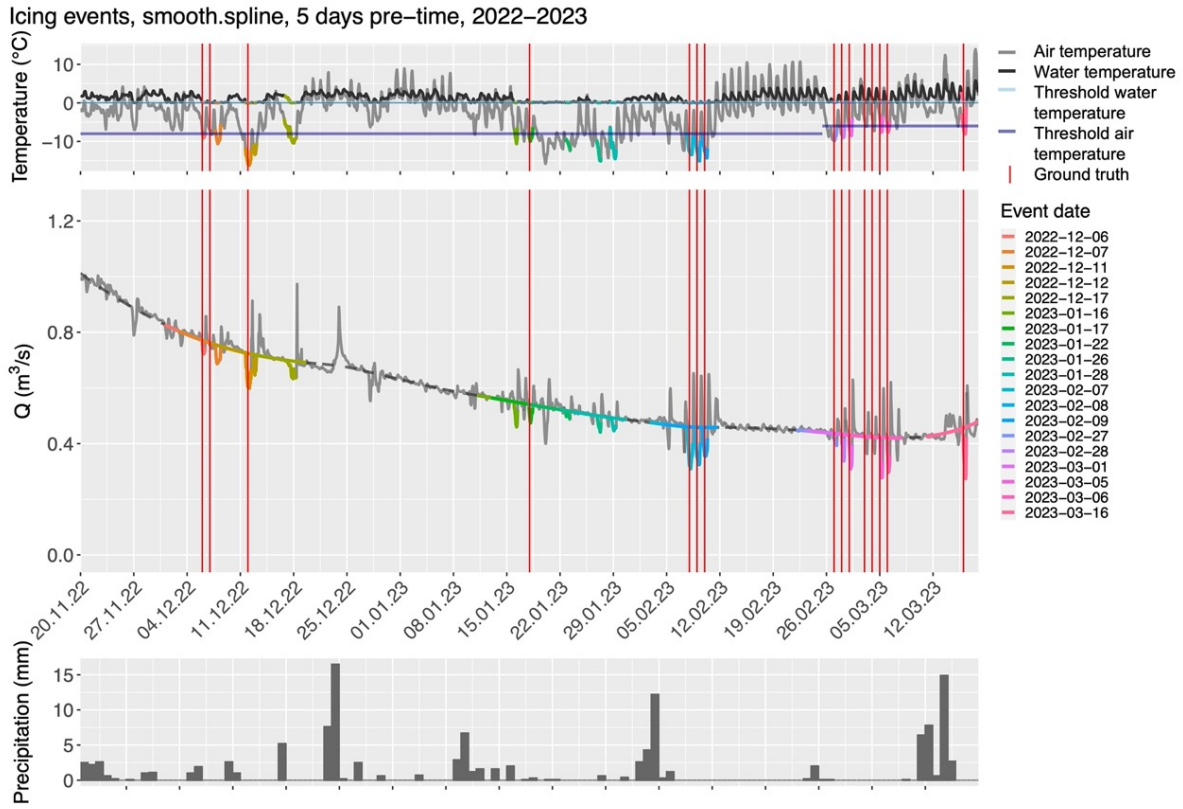

Figure 5.16: Icing events found by the Event-Finding-Algorithm in winter 2022-2023 the events detected by the wildlife camera(red lines)

Events of 2022-2023: In Figure 5.16, the temperature and discharge progression during the winter of 2022 to 2023 is detailed, including the events identified by the algorithm, the ground truth data (represented by red lines), and the average daily precipitation values. Upon analyzing Figure 5.16, it is discernible that the first event identified by the algorithm occurred on December 6, 2022, aligning with the camera imagery. Additionally, six more events were identified for which there is no direct evidence. Between February 7 and 9, three events were documented at daily intervals both by the algorithm and the wildlife camera imagery. Between February 12 and 25, both air and water temperatures increased to milder levels, which was accompanied by a noticeable absence of event identification. In the late winter, wherein a second season with less stringent thresholds was defined, the algorithm identified another five events. However, it should be noted that the camera captured two events (on March 3 and 4, 2023) that were not identified by the algorithm.

Volume analysis of 2022-2023: In the project's subsequent phase the compensation volume during each event was calculated. The obtained values are shown in Table 5.5 (Section 4.2.2.4). The retained water volume averages at 2972.96 m^3. The event with the largest retention volume occurred on February 7, 2023, where over 6200 m^3 of water was "missing" in the discharge. The duration of such events averages about 14 hours, which is slightly longer than one night. Most of these events begin at dawn (around 16-17 o'clock) and last until noon. Particularly noteworthy is the event on December 16, 2023, which had an extraordinary duration of 39 hours and thus spanned over two nights. An analysis of the discharges in the models without ice formation shows that these decrease consistently over the winter. Additionally, the compensation volumes were determined and related to the respective events. It can be observed that almost all retention volumes are larger than the respective compensation volumes, with the exception of the event on December 12, 2022, where the compensation volume exhibits a more considerable value. On average, the compensation volume is 1681.86 m^3. The maximal compensation volume was released on February 9, 2023, with a magnitude of 3345.90 m^3. The discharge rate between the retentions and the compensations varies from 0.036 m^3/s to over 0.160 m^3/s, with an average of 0.103 m^3/s.

Figure 5.17 shows the mean impounded volume compared to the predicted runoff volumes over the winter. The top two graphs illustrate the temperature and runoff histories, with icing events detected by the algorithm marked as red dots. The middle runoff graph also shows the blue dashed line of the *smooth spline* No-Ice-Model. In the lower graph, the mean impounded volumes are shown as bar plots related to the respective time in winter. The red bars represent the water impounded by ice, and the blue bars represent the expected runoff without ice. One striking observation is that the amount of water impounded by ice tends to be less in early winter than in late winter. This is also confirmed in the last column of Table 5.5, where the average early winter retention is 9.91 %. In contrast, in late winter, it is 17.16 %.

Table 5.5: Calculated volumes with the Event-Finding-Algorithm

Season	Event Start datetime	Ret. Vol. (m^3)	Ret. Duration (h)	Mean Ret. Vol. (m^3/s)	No-ice Q (m^3/s)	%	Comp. Vol. (m^3)	Mean Comp. Vol (m^3/s)	Diff. Ret. and Comp. Vol (m^3)	Diff. Ret. and Comp. Q (m^3/s)
early	06.12.22 00:00	1224.86	9	0.038	0.769	4.92	1219.27	0.031	5.58	0.069
early	07.12.22 17:00	2949.03	17	0.048	0.752	6.41	675.63	0.017	2273.41	0.065
early	11.12.22 16:00	5245.17	18	0.081	0.724	11.19	426.13	0.011	4819.03	0.092
early	12.12.22 17:00	1732.30	11	0.044	0.719	6.09	2438.08	0.062	-705.78	0.105
early	16.12.22 18:00	4072.45	39	0.029	0.698	4.16	1553.12	0.039	2519.33	0.068
early	15.01.23 23:00	2260.26	11	0.057	0.549	10.40	2128.07	0.054	132.20	0.111
early	17.01.23 22:00	1676.73	12	0.039	0.540	7.19	1126.04	0.028	550.69	0.067
early	22.01.23 17:00	891.05	15	0.017	0.517	3.19	750.29	0.019	140.76	0.035
early	26.01.23 19:00	1594.22	14	0.032	0.500	6.33	1184.76	0.030	409.46	0.062
early	28.01.23 14:00	1766.06	19	0.026	0.492	5.25	685.28	0.017	1080.78	0.043
early	07.02.23 18:00	6234.71	16	0.108	0.460	23.54	1838.84	0.046	4395.87	0.155
early	08.02.23 18:00	5908.21	16	0.103	0.458	22.37	2014.96	0.051	3893.25	0.153
early	09.02.23 18:00	4426.49	15	0.082	0.458	17.90	3354.90	0.085	1071.59	0.167
late	26.02.23 20:00	1163.97	13	0.025	0.436	5.71	1095.67	0.028	68.30	0.053
late	28.02.23 00:00	1720.92	9	0.053	0.433	12.27	1615.45	0.041	105.46	0.094
late	01.03.23 23:00	2984.76	10	0.083	0.430	19.27	2836.44	0.072	148.32	0.155
late	05.03.23 02:00	2619.81	7	0.104	0.422	24.66	2258.59	0.057	361.21	0.161
late	06.03.23 23:00	2998.28	9	0.093	0.421	22.00	2442.24	0.062	556.03	0.154
late	15.03.23 17:00	5017.00	16	0.087	0.457	19.07	2311.64	0.058	2705.36	0.145

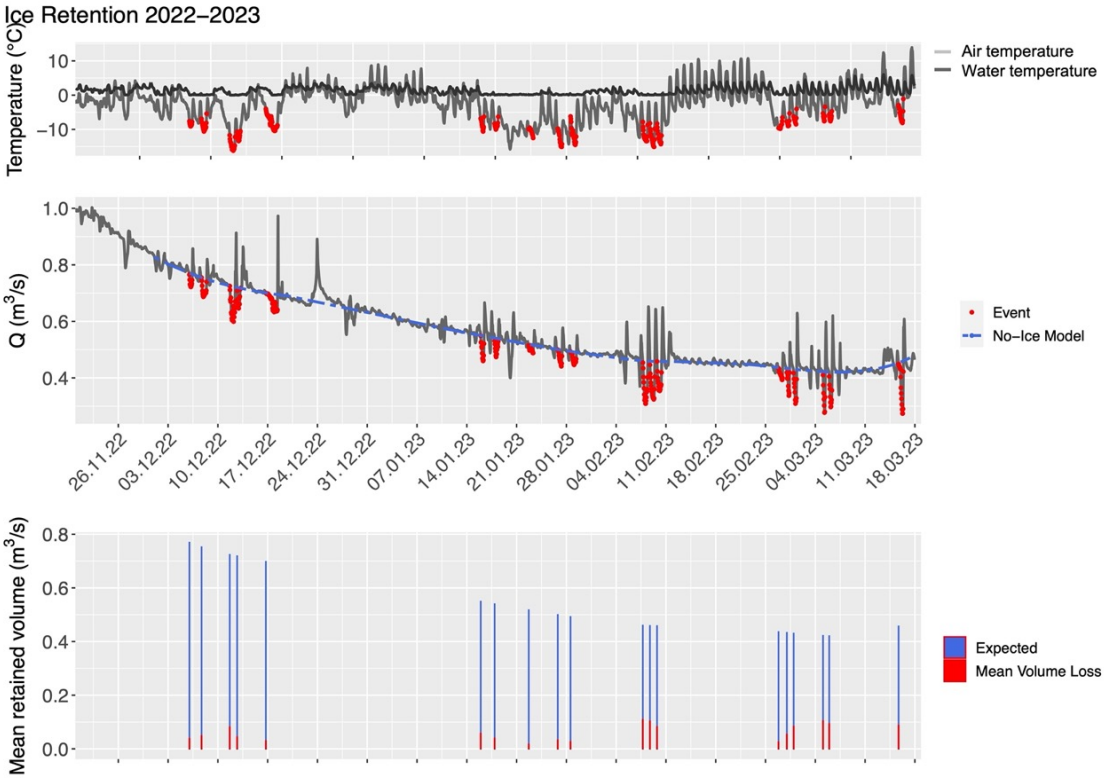

Figure 5.17: Resulting retention volumes due to ice in the Dischmàbach in comparison to the expected discharge from the No-Ice-Model

5.2.3.2 Winter 2005-2006 and winter 2021-2022

Events in the warmest and coldest winter over the last 19 years: The event-finding algorithm, which proved to be the most effective after the validation (*smooth spline*, 5 days pre-time), was applied to the data from preceding years. However, the analysis could only extend back to 2004, as continuous water temperature measurements were unavailable before this point. Table 5.6 lists the thresholds applied to all winters.

Table 5.6: Threshold values for the data from 2004 to 2022

Parameter	**Threshold value**
Air Temperature (°C)	-6 ± 0.5
Water Temperature (°C)	0.25 ± 0.05
Precipitation (mm)	0

The coldest winter occurred from 2005 to 2006, with an average air temperature of -5.37 °C, while the warmest winter occurred from 2021 to 2022, with an average winter air temperature of -1.36 °C. The events identified during these periods are depicted in Figures 5.18 and 5.19. In the winter of 2005-2006, 12 events were extrapolated, compared to 16 events in the winter of 2021-2022.

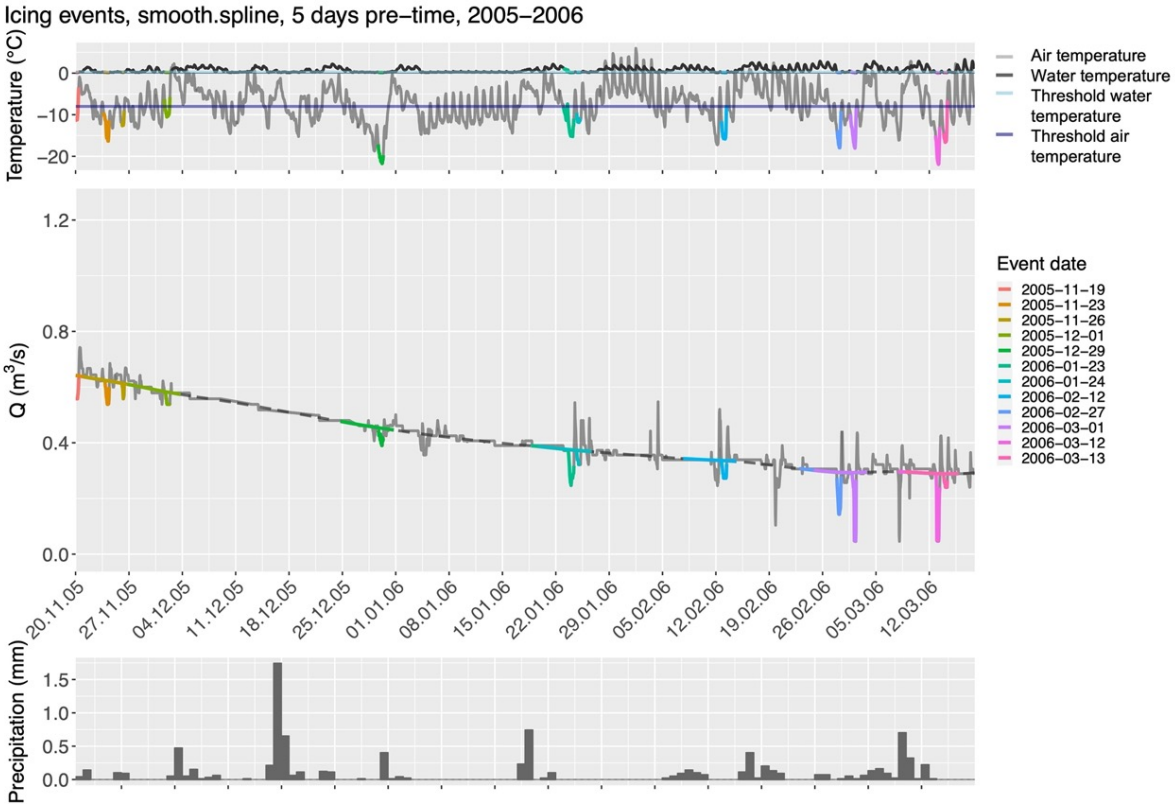

Figure 5.18: Icing events found by the Event-Finding-Algorithm in the winter 2005-2006, coldest winter between 2004 and 2023

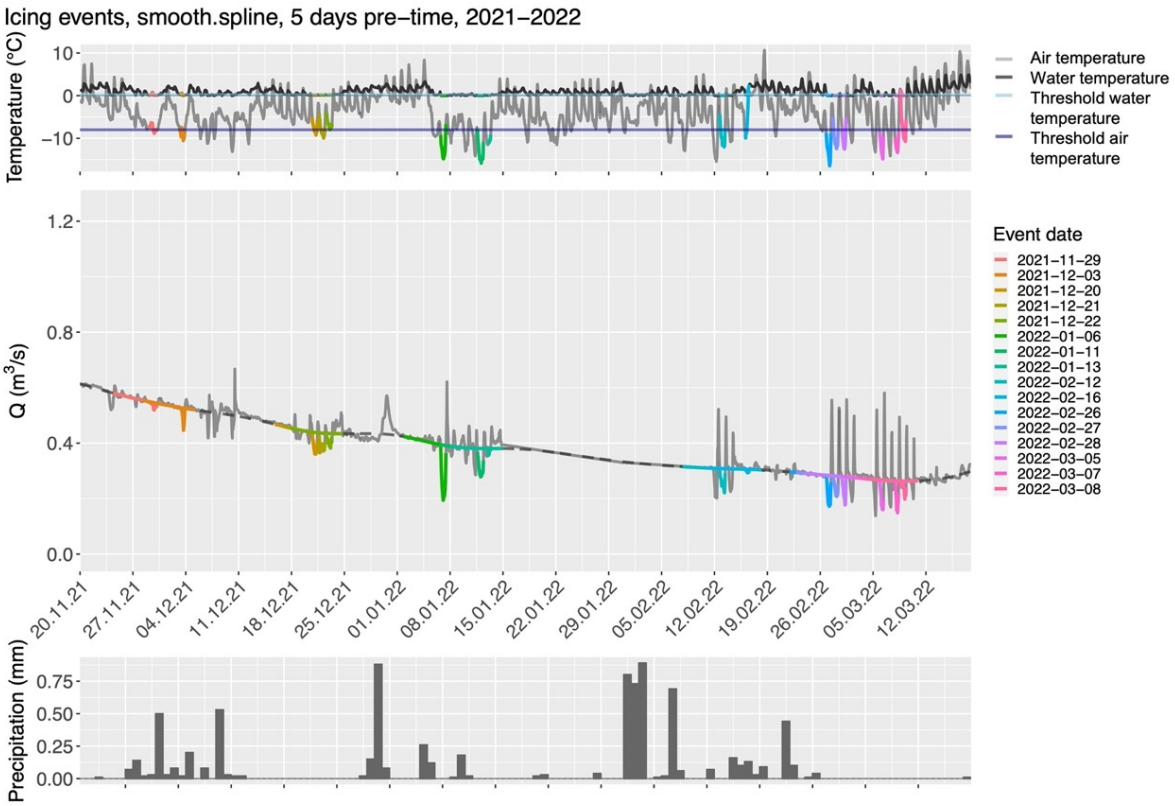

Figure 5.19: Icing events found by the Event-Finding-Algorithm in the winter 2021-2022, warmest winter between 2004 and 2023

Event volume sum: In the subsequent phase of the investigation, we summed the volumes of water retained by ice formation during the winter seasons of 2005-2006, 2021-2022, and 2022-2023. Concurrently, all the discharge values below the established *smooth spline* function curve were summed and converted to volume metrics. This summation encapsulates all the variations in discharge without differentiating the diurnal discharge patterns or influences of ice retention. Subsequently, the proportion of the retained volume was computed when juxtaposed with the volumes predicted by the No-Ice Model. Detailed outcomes of this assessment can be found in Table 5.7.

Table 5.7: Summed volumes and mean volumes retained by the ice in comparison to all negative discharge fluctuations in winter for the case study and the warmest (2021-2022) and coldest (2005-2006) winter in the last 19 years

Winter year	**Sum retained volume (m^3)**	**Sum negative volumes**	**% retained to all negatives vol**
2022/ 2023	56486.29	106482.60	53.05 %
2005/ 2006	45894.88	86928.58	52.80 %
2021/ 2022	54314.93	88729.52	61.214 %

5.3 Event-specific analysis utilizing drone images

During the night spanning February 7th to 8th, 2023, the average air temperature decreased to -13.4 °C and hovered around -6.2 °C throughout the day. The meteorological conditions were sunny, with no precipitation observed. The stream discharge exhibited fluctuations, ranging approximately from 0.3 m^3/s at night to 0.6 m^3/s during the daytime. Between 08:00 and 10:00 o'clock in the morning drone imagery was taken over the stream, capturing the ice formation in the stream. At that time, the discharge was around 0.37 m^3/s. On February 20, 2023, a second drone survey of the specified sector of the region was conducted. That morning, a mean air temperature of approximately 1.9 °C was recorded, while the nocturnal minimum temperature was about -2.1 °C. The water discharge remained relatively steady during this period, averaging around 0.45 m^3/s. The meteorological conditions on this date were consistent with those observed on February 8, 2023. The survey was carried out over a stream devoid of ice. Although snow accumulations were noted along the banks, no ice formations were visible in the stream. During both flights, Digital Surface Models (DSM) were captured. The data derived from this allowed the differentiation and classification of water levels on the respective dates of flight. These variations were apparent at specific points in the stream, aiding in mapping water retention areas. Additionally, the spatial expansion of the elevated water levels was quantified, and the increase in volume due to ice damming on February 8, 2023, was calculated respectively to the increase in water level. Figure 5.20 and 5.21 show Pool 1 and Pool 2 during icy conditions, additionally to the rise in elevation on the water surface in comparison to the water level the February 20th, 2023. It can be observed that both pools exhibit a significant water

accumulation of up to one meter or more, which is retained by a layer of ice serving as a barrier at this location.

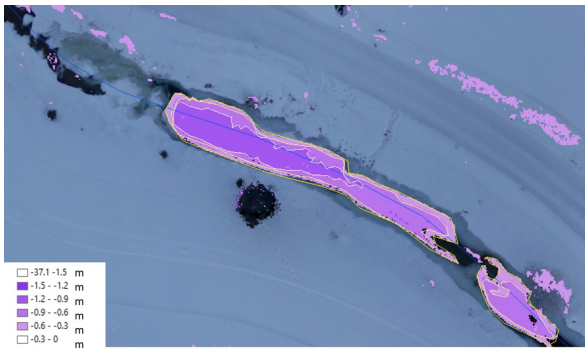

Figure 5.20: Pool 1 on the 08.02.2023, areal picture during an icing event with colored water surface elevation difference to the 20.02.2023 areal image, screenshot of the drone flight imagery

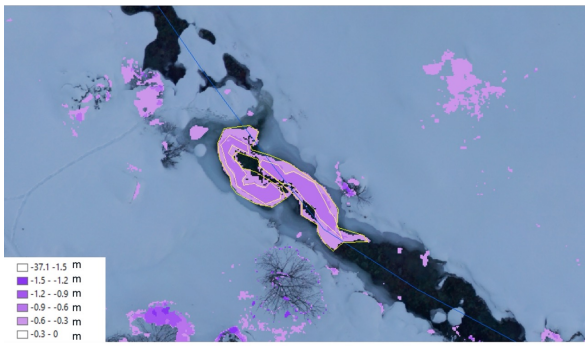

Figure 5.21: Pool 2 on the 08.02.2023, areal picture during an icing event with colored water surface elevation difference to the 20.02.2023 areal image, screenshot of the drone flight imagery

It should be noted that the analyzed area of these two flights only extends from Duchli to Chintsch Hus. For this segmentation, DSM differences were utilized.

An earlier flight on December 12, 2022, covered an area from Am Rin to Dürrboden that scanned a frozen stream. Unfortunately, no ice-free comparative flight data is available for this segment, but potential dam areas were identified by analyzing ortho-images. Therefore, the volume increase for this stream segment can only be viewed as a rough approximation, with the water surface increase estimated to be around 45 cm $\pm$ 15 cm.

It is essential to mention that no flight data collection occurred between Chintshus and Am Rin. Consequently, there are no specific data regarding ice damming in this section. Since this segment constitutes approximately a quarter of the total stream surface area, a quarter of the determined volume was added to the damming volume estimation calculations.

The following volumes result from this single event analysis:

Table 5.8: Calculated volumes of water retained due to ice with the drone flight imagery

Flight Area	**Volume (m^3)**
Duchli - Chintsch Hus	856.5 - 1553.3
Chintsch Hus - Am Rin	238.05 - 436.18
Am Rin - Dürrboden	95.7 - 191.4

Resulting in a total volume between 1190.25 m^3 and 2180.88 m^3.

5.4 Stage sensor results

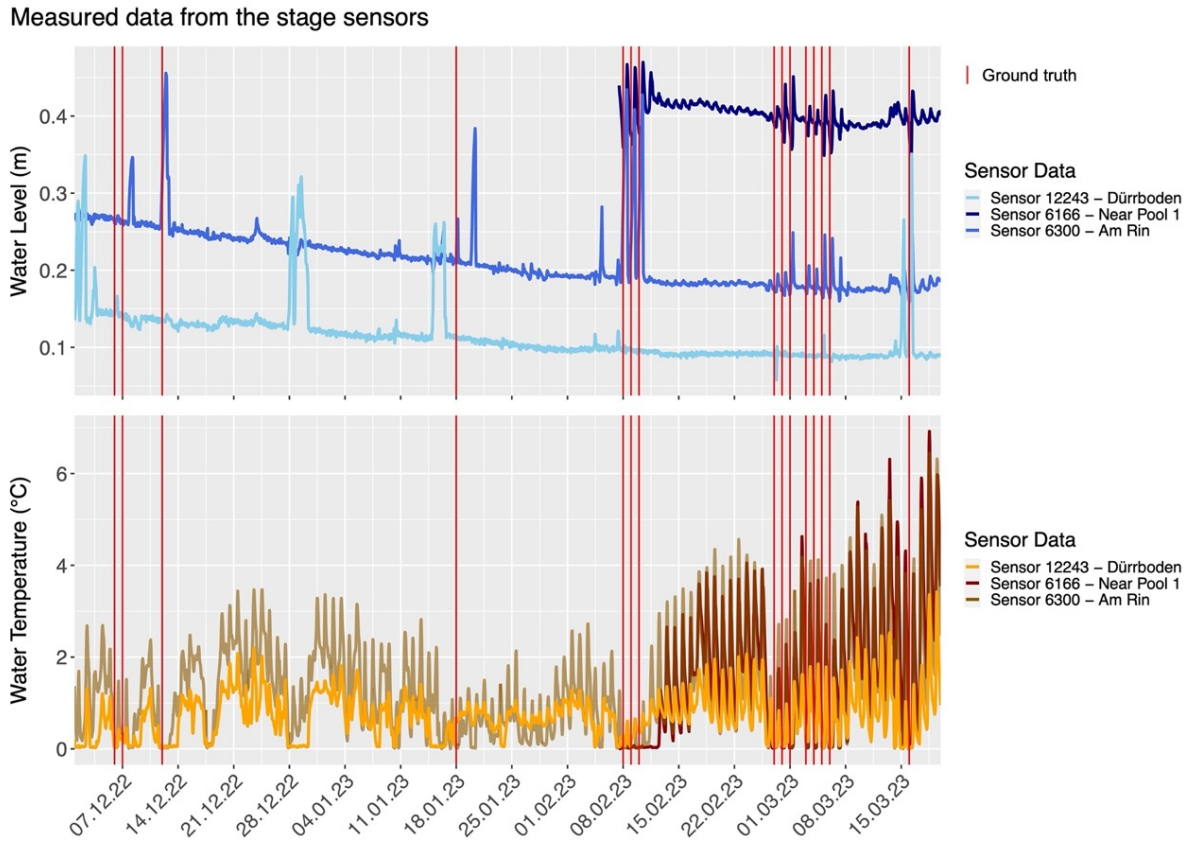

Figure 5.22: Measured water level with the Decentlab sensors in the top (Dürrboden), middle (Am Rin) and bottom (near Pool 1) of the valley

In Figure 5.22, the water level measurements along with the water temperature data, which were determined using pressure sensors, are depicted. Additionally, red lines illustrate the ground truth events captured by the cameras installed at the pools. The stage sensors 12243 and 6300, located further up in the Dischma Valley (Figure 3.1) were initially installed. Although both level measurements indicate peaks in the water level curve, it can be noted that these pressure increases do not exhibit preceding retention phases, as found, for example, in the hydrograph of the FOEN station in Kriegsmatten. Upon closer inspection of the simultaneously captured water temperature data, however, it is noticeable that they are very close to the 0 °C mark.

In contrast, the water level graph of the later installed stage sensor number 6166 displays both retention and compensation phases, especially when the water temperature is near 0 °C. This sensor, situated considerably lower in the valley at a bridge near Pool 1, presents a more nuanced picture of the hydrological dynamics in this region.

Chapter 6

Discussion

In the preceding sections, the ice formation processes in the Dischmàbach were examined in detail. This encompassed a comprehensive analysis of the stream morphology concerning ice formations and a thorough investigation of the stream's hydrograph. The goal of these investigations was to gather the necessary data to answer the research questions. In the following chapter, a careful discussion and interpretation of the obtained results will be conducted and brought in a broader context of the existing literature.

As a starting point for this discussion, it is perhaps worth highlighting the confirmed existence of the presumed temporary ice formations, which exert a significant influence on the discharge. These were clearly demonstrated and documented during the field campaign at the Dischmàbach between November 2022 and March 2023.

6.1 Morphological analysis of stream ice formation dynamics

6.1.1 Stream morphology

The stream morphology, identified by the scientific community as a decisive factor for the formation of certain stream ice formations, was investigated (Turcotte and Morse, 2013; Stickler and K. T. Alfredsen, 2009; Nafziger et al., 2017; Hirayama, Yamazaki, and Tao Shen, 2002). The morphological study of the stream in relation to winter ice formations revealed that the stream undergoes substantial variability with regard to width and gradient, showcasing varying wide and narrow, as well as steep and flat areas. In general, it is observed that, the stream width increases and the gradient decreases going downstream the valley; demonstrating a typical flow behavior of an alpine stream that springs from steeper terrains and winds down a flattened valley (Figure 5.1). When observing the ice formations noted, it becomes clear that these cannot be visually attributed to specific location formations (Figure 5.1). However, by comparing the mean values of stream width and slope of areas rich in ice and those less ice-covered, a difference can be stated. This indicates that the sections near ice dams are, on average, flatter

than the ice-free areas and that the stream width generally increases (Table 5.1). A potential reason for this observation might be the manual mapping method employed. This technique pinpointed sections in the stream where water accumulates, typically found directly behind an ice dam. This finding seems to corroborate existing theories in the literature, suggesting that ice dams predominantly form in stream stretches featuring a pool-and-step structure (Turcotte and Morse, 2013; K. Alfredsen, Stickler, and Pennell, 2006; Hirayama, Yamazaki, and Tao Shen, 2002). As a result, the previously mentioned pools — which generally exhibit a wider breadth and more flat slope compared to the "steps" — serve as the main sites for water retention, further substantiating the observed data. Typical riffle or step-and-pool formations were also observed during the field inspections.

6.1.2 Pool morphology

Ice-rich locations: Further investigations, on a more local scale, particularly concerning conditions at Pool 1 and Pool 2, showed many ice dynamics over the case study winter. Both pools were photographed at regular intervals during the winter of 2022-2023. This provided excellent documentation of stream ice dynamics at these two locations and was confirmed by the water temperature loggers (in the case of Pool 1), which measured 0 °C water during the observed events (Figure5.6). Both anchor ice and slush ice were detected in both pools, and it was clear that they were causing water accumulation behind the iced zones. In addition, the specific morphology at these locations was described in detail. Both pools present a shallower jammed zone and a steeper step formation. As a result, the observed water velocity increases slightly at the steeper sites and transitions to an area characterized by turbulent flow conditions. Just between the flat and steeper zones, anchor ice formed between the boulders and built up during certain cold nights to the point where it could block the water. In the morphology graph of the sites, it can be seen that, especially in Pool 1, the observations of ice formation are behind the morphological stage (Figure 5.2 and 5.7). Thus, these field data also confirm the characteristics already described in the literature (Turcotte and Morse, 2013; Stickler and K. T. Alfredsen, 2009; Nafziger et al., 2017; Hirayama, Yamazaki, and Tao Shen, 2002). Additionally, two water temperature loggers were installed in Pool 1. The resulting data indicate that the sensor positioned closer to the morphological step records longer time periods where the temperature remains at the 0 °C threshold. This further substantiates the theory that anchor ice must have formed at this location. It can be concluded that on some nights during the past winter, water accumulated and built up ice at these sites during a supercooling phase (Boyd, T. Ghobrial, and M. Loewen, 2023; Boyd, T. Ghobrial, M. Loewen, et al., 2022). Another remarkable phenomenon observed at Pool 1 is an overhanging ice cover spanning the entire course of the stream. It is assumed that this formed in the advanced winter, probably around the beginning of February. This phenomenon is also addressed by K. Alfredsen, Stickler, and Pennell, 2006, who explained that more stable ice covers can develop as a result of temporary anchor ice formations later in the cold season. Even if the anchor ice layer breaks up due to intense solar radiation, a more

solid ice cover can remain. This corresponds well with the observations of the ice cover at Pool 1 and offers a plausible explanation for the conditions there (Figure 5.4).

No-ice location: Unlike Pool 1 and Pool 2, no ice was detected at Pool 3 throughout the winter. This site has a wider structure than the average stream channel, and unlike the other two sites, the water here flows over a small waterfall into a larger pool, as illustrated by the morphograph. Although the temperature logger recorded some very low temperatures early in the winter, no water logging was observed at this site. There are two plausible explanations for the absence of anchor ice at this location: First, upon examining the summer orthoimages of the site, it is evident that a side stream flows into the Pool 3 location. This water could originate from a groundwater reservoir, hence being insulated from freezing below ground. The warmer water from this side stream might inhibit supercooling and prevent the formation of slush ice and anchor ice (see Figure 5.12). However, the precise temperature of this side stream's water and whether it emerges from an underground source remain unverified. Secondly, the morphological structure of this site could be a factor. Water flows over a small waterfall into a more expansive basin, as opposed to the configurations at Pool 1 and Pool 2. The pronounced turbulence caused by this small waterfall might induce enhanced mixing, which could be too intense for supercooled conditions to arise, as suggested by Daly, 2013.

6.1.3 Summed up discussion points to the morphological analysis of stream ice formation dynamics

Summing up the results from the morphological analysis in connection to temporary ice formation the data from the Dischmàbach demonstrate that the stream's morphological features profoundly influence ice formation patterns. Particularly, regions with a noticeable transition between slow and fast currents, characterized by morphological steps and emerging boulders, are more susceptible to anchor ice formation. According to classifications by Turcotte and Morse, 2013, the Dischmàbach meets the essential prerequisites found in streams prone to temporary ice dam formations, owing to its geographical incline and climatic conditions. Consequently, its morphological diversity makes it an exemplary site for investigating the different ice dynamics that can occur in alpine regions. This aligns with the research by Turcotte and Morse, 2013 and Hirayama, Yamazaki, and Tao Shen, 2002, reinforcing the hypothesis that the Dischmàbach serves as a significant exemplar of streams capable of developing temporary ice dams and their associated dynamics.

6.2 Event analysis

6.2.1 Analysis of the Event-Finding-Algorithm Efficiency and Event Identification

6.2.1.1 Event characterization:

In the present study, a ground truth was established for the Event-Finding-Algorithm based on the image frequency captured using wildlife cameras. To create a valid data foundation, the observed events in the images were correlated with the air and water temperature and precipitation data from the FOEN station in Kriegsmatten. This correlation facilitated the definition of various threshold values, which hypothetically represent the maximum possible temperatures and precipitation values at which ice formations can occur. It is important to note that this process was specifically developed for the area under investigation, which could potentially limit the general transferability of the algorithm. The threshold values established in this study can now be compared with those of further studies, as shown in Table 6.1.

Table 6.1: Comparison of air temperature thresholds observed in different field studies investigating ice formations in streams

Study location and measuring period	**Air Temperature Threshold (°C)**	**Reference**
Dischmàbach, Dischma Valley, Switzerland between 2022-2023	-8 and -6	*Own field campaign*
North Saskatchewan River and Peace Rivers, North Saskatchewan and Alberta, Canada between 2016-2017	-5.4	Boyd, T. Ghobrial, and M. Loewen, 2023
Hokkaido, Japan between 1996-1997	-10	Terada, Hirayama, and Sasamolo, 1999
South West River, Newfoundland, Canada between 2005-2006	-15	K. Alfredsen, Stickler, and Pennell, 2006

The analysis of data from other studies indicates that all observed values exhibit temperatures in the negative range, although these vary considerably. This suggests that the specific conditions depend heavily on the respective environment, which is why an individual consideration for each area is recommended in order to make more precise predictions.

6.2.1.2 Event-Finding-Algorithm performance:

The performance of the Event-Finding-Algorithm was assessed by comparing the number and the consistency of the events identified by the algorithm with the observed ground truth events. The analysis indicated that the *smooth spline* No-Ice-Model, with a period of 5 days, exhibited the best performance. A comprehensive concordance between the observed events and the events identified in the hydrograph was observed, indicating an overall high efficacy of the Event-Finding-Algorithm.

Even though the *smooth spline* No-Ice-Model showed the best performance compared to the *exponential decay* No-Ice-Model it has to be stated that this approach also brings a notable drawback. The *smooth spline* is a function that fits a statistical smoothing to the data and finds the best trade-off between the smoothing and goodness of fit (Eubank, 1999). In this case, the *smooth spline* No-Ice-Model does not distinguish between various water inputs in the stream. It computes the volume both below and above the estimated no-ice discharge line without differentiating between permanent ground flow and temporary flows such as snowmelt or precipitation. As a result, the model tends to overestimate the ground flow contribution and the associated retention volumes on the graph. On the other hand, the *exponential decay* No-Ice-Model operates on the principle of a recession function that ideally captures the optimal low-flow conditions in the riverine environment (Tallaksen, 1995). Despite its theoretical premise, this model has manifested a suboptimal performance when juxtaposed with the *smooth spline* No-Ice-Model. Furthermore, it's predicated upon a relatively simplistic computational framework that fails to encapsulate the complex recessional behaviors observed in stream systems (Tallaksen, 1995). In light of these findings, it is pertinent to acknowledge that the *smooth spline* No-Ice-Model serves as a valuable instrument in identifying events within the hydrograph, whilst also offering preliminary estimations concerning retention and compensation volumes. However, a refined comprehension of hydrograph separation techniques is warranted. This would facilitate the development of a model that adeptly portrays the underlying ground flow dynamics, paving the way for more realistic volume calculations that closely mirror actual conditions.

6.2.2 Evaluation of the Events and the Impounded Water Volumes

6.2.2.1 Winter 2022-2023

Evaluation of the events: The Event-Finding-Algorithms found a total of 19 events during the winter between 2022-2023, with 13 matching the wildlife camera ground-truth (Figure 5.16). Six events were found by the algorithms but not proved by the wildlife camera pictures. They lay between the end of December 2022 and February 05, 2023, when the camera had malfunctioned and thus did not record anything. By comparing those six events to the meteorological conditions, they are plausible as air and water temperatures dropped to very low degrees. The event gap between December 24, 2022, and January 10, 2023, can be attributed to the relatively

mild temperatures during this span, coupled with a precipitation event in the form of rain on December 24, 2022. On the contrary, the wildlife camera registered two events (the 3 and 4 or March 2023) while the algorithm did not mark them. It could be attributed to the fact that they are minimal oscillations and thus not significant enough to be recognized.

Evaluation of the events volumes: The recorded mean of impounded volume per event during the winter of 2022-2023 resulted 2973 m^3. The starting time and duration show that the events often span between dawn to noon the following day, potentially illustrating a pronounced diurnal cycle. Ice processes thus, influenced by nightly decreases in temperature and decrease in incoming short radiation. This phenomenon is well-documented in literature, with studies such as those conducted by Boyd, T. Ghobrial, and M. Loewen, 2023 noting significant variations in river discharge volumes in accordance to daily temperature and radiation fluctuations.

Upon comparing of the mean retained discharge per event with the expected discharge from the No-Ice-Model, a range between 3 % and 25 % in the "missing" water volume is observed over the winter. This variance is illustratively represented in Figure 5.17. A salient observation from the data indicates a pronounced augmentation in water retention from the onset to the latter part of winter. This trend might suggest a cumulative effect stemming from the successive layering of ice as the winter season advances. This hypothesis aligns with findings documented by K. Alfredsen, Stickler, and Pennell, 2006. In their research, as winter persists, a suspended ice cover begins to manifest over river segments. During colder nocturnal periods, temporary ice building up in the riverbed can amalgamate with this overhead ice layer, potentially obstructing the river channel and bolstering its water retention capacity. Such a phenomenon of a suspended ice cover was also discernibly evident at the research location, Pool 1, as depicted in Figure 5.4.

The mean compensated volume throughout the winter of 2022-2023 was determined to be 1681.88 m^3. Intriguingly, it is inferior to the retention volume, indicating that the entirety of the water retained by the ice is not immediately reintroduced into the stream post-retention. A potential reason for this observation could be attributed to several factors such as miscalculations or physical processes like physical trapping, percolation to groundwater or ecological factors. Not only temporary ice formations like slush ice or anchor ice form in the stream but also more persistent ice formations, like ice covers or ice at the riverside (K. Alfredsen, Stickler, and Pennell, 2006). This could thus physically trap the water which is then missing during the release of the compensation discharge. Furthermore, water can percolate through the streambed to the groundwater reservoir.

6.2.2.2 Winter 2005-2006 and Winter 2021-2022

Evaluation of the events found in 2005-2006 and 2021-2022: In a subsequent phase of the project, the Event-Finding-Algorithm was applied to the data of the warmest and coldest winters of the last 19 years to assess the applicability of the algorithm in analyzing diverse data

sets. The analysis demonstrated that during the coldest winter (2005-2006), twelve events were detected, whereas in the warmest winter (2021-2022), sixteen events were identified. Notably, the warmer winter exhibited a higher number of events, which might not be what it is expected. Upon closer inspection of the discharge and temperature graphs (Figure5.18 and 5.19), however, it is clear that the discharge in December 2005 and January 2006 remains completely static and unchanged even if the air and water temperature drops to very frigid levels. This could be attributed to manual corrections of the data by the FOEN. The FOEN data up until early 2022 had already been scrutinized and corrected for possible errors by the authorities. However, during a conversation with A. Kohler, representative of the Department of Hydrology from the FOEN (Kohler, 2023) noted that strong fluctuations in the discharge graphs were often deleted since their plausibility was questioned. Consequently, the sensors at the measuring station were often misinterpreted, and this "cleaning process" was applied even more rigorously in the past. This observation is consistent with a recently published paper by Strohmenger et al., 2023. The paper suggests that during low-flow conditions, various artifacts and data patterns are often removed from the records during the data correction process. These patterns might actually correspond to real natural phenomena that are not yet fully understood. As a consequence of the corrections, these phenomena are mainly overlooked since the adjusted data no longer display them. Despite the positive results, it must be taken into account that the events identified by the algorithm in previous years are unfortunately not empirically verifiable, as no corresponding image materials are available. However, conversations with the local population provide valuable qualitative evidence that stream glaciations did not only occur this winter, but were already observed in previous years (Frankhauser, 2022b). These statements are supported by consistent patterns of fluctuation that are also evident in hydrographs from previous years, which can serve as indirect evidence of the reliability of the algorithm.

Evaluation of the summed volumes: During the investigation, water volumes retained by ice across three winter seasons were summed, and discharge values below the *smooth spline* curve were aggregated. The comparison with the No-Ice Model allowed for the calculation of the retained volume's proportion. It resulted that for all three winters the negative volumes were more than the half caused by ice retention. For the winter of 2022-2023, 53 % of the negative volume was ascribed to ice retention. In the colder winter of 2005-2006, 52.80 % of the negative volume was due to ice-induced water retention and in the warm winter of 2021-2022 it reached 61 %. One might expect that colder winters would inherently result in more freezing events, thereby leading to a higher percentage of retained volume over the winter. However, when comparing the three selected winters, the opposite seems to be true. This prompts the question: does a generally warmer winter necessarily preclude the possibility of intermittent temperature fluctuations that could still lead to temporary ice formations? It's worth noting that the manual corrections made to the 2005-2006 data could have contributed to this discrepancy, making it challenging to discern a definitive pattern.

6.2.3 Summed up discussion points to the event analysis

Summed up the Event-Finding-Algorithm worked well as a first approach to study the anomalies during low-flow in the Dischmàbach. It identified most of the events and it gave a first estimate of how much water is retained during the temporary damming due to ice. Even though, the Event-Finding-Algorithm is based on discharge behavior and meteorological data. However, as described in the literature and from the field observations, the riverbed morphology has a significant role in the ice formations. Thus, the Event-Finding-Algorithm is not enough to determine if ice is building in a stream as the morphology also has to be considered. This might also explain why not all the events are found by the algorithm that was observed in the cameras.

6.3 Results from drone images and comparison to the Event-Finding-Algorithm results

The event-specific analysis utilizing drone images focused on the ice formation event between February 7 and 8, 2023. In this analysis, a retention volume of approximately 1990 m^3 to about 2181 m^3 was calculated. In parallel, the Event-Finding-Algorithm calculated a volume of 6234.71 m^3 for the same period, which is about three times the volume analyzed using drone images. It was originally expected that both calculations would yield a similar volume. However, it must be considered that the drone flight analysis likely underestimated the retention volume for several reasons. First, the water height areas were manually outlined, which is prone to errors due to oversight. Secondly, a detailed analysis of the ice-rich and ice-free areas was only possible for half of the river area. The other half of the river was only flown over once and on a different day. Although it can be assumed that the icing locations should be the same, the volume differences could vary considerably, especially since the flight datetime of the first flight was at the beginning of the cold period. A third possible underestimation arises from the missing data about the third quarter of the river, where no data collection took place due to organizational and time constraints. Subsequently, it is assumed that the algorithm volume analysis of the hydrograph using the *smooth spline* No-Ice-Model possibly caused an overestimation of the retention volume. This is because the *smooth spline* statistically considered the flow course over the winter and thus, not only groundwater flow conditions could prevail in the river but also snow melt or other water inputs. These uncertainties and assumptions could bring the two volume calculations closer to each other, and thus the results are not as far-fetched as they may initially seem.

Consequently, it can be concluded that the drone flight analysis is subject to some uncertainties but still represents a very effective method for mapping these ice formations in the river.

6.4 Evaluation of the stage sensor results

The data from the water stage sensors revealed interesting patterns. The sensors at Dürrboden and Am Rin indicated a rise in water levels during frigid water and air temperatures. However, they did not display a retention phase followed by a compensation phase. In contrast, the sensor near Pool 1, located further down the valley, exhibited patterns similar to the FOEN station in Kriegsmatten. One hypothesis is that the sensors positioned higher up in the valley may have frozen over the winter. This freezing could have exerted added pressure on the sensors, leading to inaccurate water level readings. Another possibility is that these sensors, being further upstream, don't capture the retention signal across the entire stream. If only a few locations upstream are causing water retention, the sensors might not detect a significant retention signal. On the other hand, the sensor lower down the valley can capture this retention signal, as it aggregates the water volumes held back by ice at various elevations. An additional observation is that the three locations don't freeze simultaneously. This suggests that ice doesn't form consistently across the entire river at the same time or under identical conditions. There's considerable variability, which may also introduce uncertainties when determining retention volumes.

6.5 Answering the research questions

The gathered interpretations and observations in the discussed results are thus used to answer the initial research question, starting from the two subquestions.

RQ1.1 *Where along the course of the Dischmàbach does ice formation predominantly occur?*

In alignment with existing literature, it was observed that both temporary and persistent ice formations typically occur at specific locations along the Dischmàbach, particularly where the river morphology transitions from a wider section to a steeper and narrower section and the flow is rather turbulent. This phenomenon was substantiated through observations at both Pool 1 and Pool 2. Determining whether this pattern is pervasive throughout the entire river remains challenging based solely on a rudimentary analysis of river width and slope. Notably, at locations where water retention is augmented during icing events, resulting in a heightened water level compared to ice-free conditions, the gradient is observed to be gentler and the width slightly larger. This has led to the hypothesis that these locations might correspond to small basins, succeeded by a morphological step. This assumption is grounded in the concurrence of the data with existing scholarly insights. However, to make definitive conclusions, a more comprehensive investigation into the river bed topography is necessitated.

RQ1.2: *Can the water volumes retained by these ice formations be quantified?*

The volume of water retained due to ice formation was quantified through a comprehensive

hydrograph analysis, complemented by the implementation of an event-detection algorithm. This methodological approach was substantiated by field observations confirming the role of ice in water retention. Data from strategically placed pressure sensors, which monitored water levels and exhibited patterns congruent with ice formation, further reinforced this hypothesis (Figure 5.22). Consequently, an initial volume quantification was achieved. Nevertheless, it's crucial to address the limitation of the No-Ice-Model previously mentioned (Section 6.2.1), which does not differentiate between water sources. It is plausible that the volume recorded during a retention event comprises a blend of water held back by ice obstructions, water physically encapsulated as ice, melt water from snow, and direct precipitation.

RQ *How does ice formation influence the patterns and characteristics of winter discharge behavior in the Dischmàbach near Davos during the winter of 2022-2023?*

Results from all three methodological approaches show that the discharge of the Dischmàbach is influenced by temporary and permanent ice formation. Over the winter of 2022-2023, multiple ice formations have been monitored and observed. And the results show that ice formation can reduce the river's effective flow area, thereby influencing the retention volume and potentially altering the flow velocity and other hydraulic parameters.

6.6 Uncertainties

Uncertainties during fieldwork data collection: During field measurements, several irregularities and malfunctioning occurred.

- One of the water temperature loggers in Pool 3 did not record any measured data due to malfunctioning
- The wildlife cameras had some data gaps as the batteries ran out or different malfunctions occurred.
- During drone flight measurements, organizational and temporal issues allowed to fly only 5 times over the winter. Furthermore, drone images were captured without control points, which increases the insecurities of the DSM images in the x-y-z direction.
- The selected locations of the water pressure sensors at Dürrboden and Am Rin proved to be suboptimal. During the winter months, these locations regularly froze over, resulting in incorrectly high-pressure recordings.

Uncertainties of the morphological analysis of stream ice formation dynamics: The main uncertainties of the morphological analysis method result from the used data. The elevation models have a maximum resolution of 0.5 m, which limits the representation of some more precise

features. Also, the elevation model captures the water surface rather than the topography of the riverbed, which is a potential source of variation. Additionally, errors may have occurred in the determination of the river edges, as these were manually captured using Swisstopo orthoimagery and drone imagery, leaving room for potential inaccuracies. The centerline of the river was also defined by the river margins, which exposes it to the same uncertainties.

Uncertainties of the event analysis: Insecurities arising from the results of the event analysis have multiple origins. The first pertains to the methodological approach, which can be viewed as subjective given that the ground truth was established through a visual analysis of images. Additionally, oscillations in the Dischmàbach winter hydrograph were presumed to result from ice formation in the stream before conclusive evidence was provided, suggesting a more inferential methodology. Moreover, the FOEN data used from 2022-2023 had not yet been adjusted for potential artifacts and measurement errors from their instruments. Similarly, the No-Ice-Model presented certain drawbacks, as already discussed in Section 6.2.1.

Uncertainties of the event-specific analysis utilizing drone images: Uncertainties in calculating the retained volume during individual events captured by drone flights primarily arise from the unaccounted overflow between Chitnsch Hus and Am Rin. Furthermore, the areas extrapolated from the images taken during the flight over Am Rin to Dürrboden lacked a comparative flight conducted under non-icy conditions and with similar discharge scenarios. An additional source of inaccuracy stems from the extrapolation of the impoundment area, as this was delineated manually around the polygons identified by the DSM difference.

Chapter 7

Conclusion

This thesis aimed to understand better the influence of stream ice formation in the alpine stream Dischmàbach winter runoff through an exploratory analysis. A morphological stream characterization with a focus on three specific locations was combined with hydrograph analysis and a drone survey. The combination of own collected data during the field campaign in winter 2022-2023 and the data collected by an official measuring station from the FOEN was used to implement different methodological approaches.

A morphological study was conducted to gain a deeper understanding of where the stream icing occurs. The morphology of the river or stream plays a crucial role in ice formation, as morphological variability strongly influences ice processes. It has been found that formations of steps and pools and turbulent flow conditions are essential for ice formation in the stream. If the stream flows too steeply or its course is too uniform, these conditions do not occur.

In addition, the volume of water retained during an icing event was studied. Last winter's hydrograph (2022-2023) was analyzed in detail and evaluated using a newly developed algorithm called the Event-Finder-Algorithm. This algorithm identifies specific events in the graph based on air and water temperature thresholds, as well as precipitation and hydrograph histories. Using a function that shows the course of runoff without ice formation (and thus, there are no fluctuations in the graph), the volume of impounded water could be determined as well as the compensation volume, which is released when ice formation break. The calculated volumes indicate that a significant volume of water is retained during winter icing - about half compared to all negative deviations. The Event-Finder-Algorithm was applied to both the warmest and coldest winters in the last 19 years of the Dischma Valley. This demonstrated its capability to identify events even in varied datasets. A significant observation from this application was the apparent strong correction in past data, which seemed to have eliminated potential discharge oscillations caused by river icing. This assumption was later confirmed during a meeting with a representative from the FOEN measurement data.

A single event in winter was studied in detail by a drone flight mapping the stream. In particular,

icy spots with high retention capacity in the stream were marked.

From our investigations of the Dischmàbach, it's evident that intermittent icing events exhibit distinct hydrological patterns. These icing events lead to a reduced effective flow area of the stream, influencing the retention volume and potentially altering flow velocity and other key hydraulic parameters. However, determining the exact impact of these icing events on winter runoff behavior poses a challenge due to various interacting factors. To fully understand and quantify these dynamics, a more detailed research approach incorporating advanced techniques and measurements is recommended. In conclusion, this hydrological research serves as a crucial initial step toward a deeper understanding of phenomena that impact various water management tasks, risk assessments, and water usage. It demonstrated that minor data anomalies can be attributed to natural phenomena that were previously overlooked. Further studies in other alpine catchments would be valuable, aiming to establish general river ice behavior in this region and climate. Additionally, it would be insightful to ascertain why certain rivers may not exhibit ice-induced oscillations in their data.

7.1 Main achievements

- **Mapping of ice-retention locations:** The morphological analysis and the drone flights over the stream allowed the identification of locations prone to temporary ice formations.
- **Temporal event identification and quantification:** Development of an algorithm capable of extrapolating ice events in a stream's hydrograph. This includes a preliminary approach to defining both the retained volume and the compensation volume.
- **Identification of significant data pattern which was neglected before:** Identification of a specific pattern in data of hydrological importance. This pattern was previously considered a measurement error by the FOEN but is actually a real phenomenon.

7.2 Possible outlooks

Based on the findings in this thesis, the following topics and approaches can further be implemented:

- The Event-Finding-Algorithm could be further refined and applied to hydrographs from other river and creek catchments. Integrating a more advanced No-Ice-Model may enhance the hydrograph separation process, leading to improved predictions of a river's recession behavior.
- The detection of ice-induced anomalies in the hydrograph warrants further exploration, especially in the context of hydrological forecasting models. It would be insightful to

assess whether these models inherently account for runoff variations stemming from ice formations. Alternatively, incorporating these ice-induced variations as input parameters might enhance the predictive accuracy of these forecasting models.

- The Event-Finding-Algorithm can be applied to historical raw data from the stream. By doing so, it might identify additional discharge oscillations and potentially offer corrections.

- The analysis of winter discharge oscillations induced by ice formations presents an opportunity for refinement in legislation concerning water usage during low-flow conditions. Current regulations predominantly focus on the Q_{347} metric, derived from daily means, which overlooks transient fluctuations (BUWAL, 2000). Consequently, these guidelines may not account for moments when water discharge dips below the Q_{347} due to temporary ice formations. While further research is essential, it's crucial to be cognizant of this aspect when formulating or revising water management policies.

- The impact of discharge oscillations on fish habitat in small alpine rivers warrants investigation, especially concerning how these temporary reductions in flow might influence fish behavior. Such fluctuations could potentially affect migration patterns, breeding habits, and foraging activities, thereby having broader implications for the overall health and sustainability of these aquatic ecosystems (Prowse, 2001).

- The inclusion of climate change and global warming would also be a further approach. Expected rising temperatures in the Alps lead to the reasonable conclusion that less ice will form in the alpine rivers and streams. Even though those do no rule out very cold periods and extreme climate variability (K. Alfredsen, Bridges, et al., 2022), suggesting that ice formation could thus be more difficult to predict.

Chapter 8

Excursus

During the field study, various encounters arose with residents of the valley who expressed interest in the ongoing measurements and investigations. Exciting conversations about wildlife and historical events enlivened the discussions Frankhauser, 2022a. Regarding the formation of ice formations in the stream, most residents agreed that the moon and its relationship to the elliptical orbit around the earth determine whether or not ice forms. During the so-called "*obsigend*" (ascending) phase of the moon, ice forms in the creek when it is moving upwards in its elliptical orbit. In contrast, ice decays during the moon's "*nidsigend*" (descending) phase and does not form again until the next "*obsigend*" phase occurs (SpaceWeatherLive, 2023). The statements have aroused our interest because residents repeatedly presented them. These narrations are best explained in the book *Dischmatal.Bilder, Geschichten, Rezepte* by Walter-Degener, 2017:

"*Under special conditions, a spectacular natural phenomenon can be observed at Dischma Creek. It has to be rather cold, though, and the moon has to move in its ascendent (obsigend) phase. At this point, the water surface freezes over, with the rising water flowing over it again, which in turn freezes and so on. Since this lunar phase lasts fourteen days, the process of high water and the simultaneous icing over is repeated several times, making the surface appear elevated.*"

So far, the moon's influence on the river has not been mentioned or considered in the scientific literature. Furthermore, When comparing the identified icing events with the lunar calendar, no clear correlation could be found (Figure 8.1)

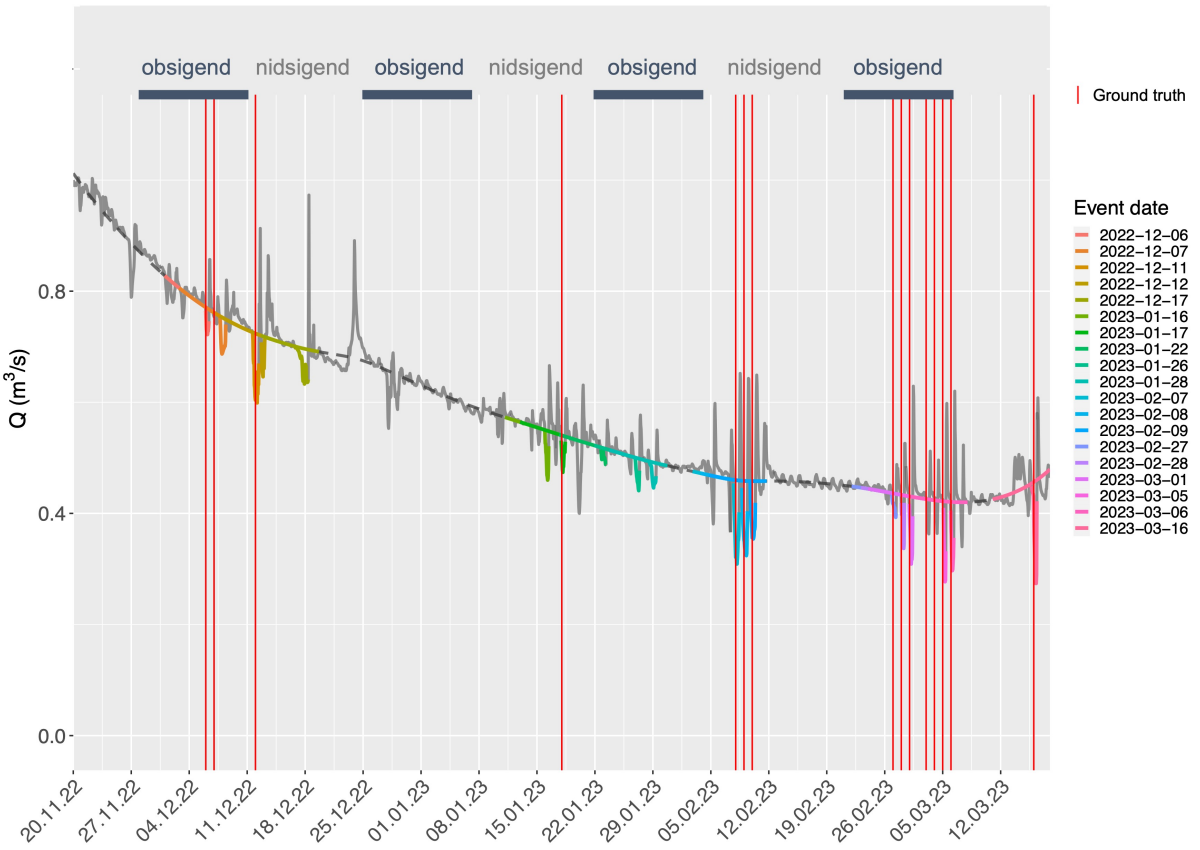

Figure 8.1: Discharge graph with the found event by the algorithm and the observed event with the wildlife camera (red line) and the moon phases (SpaceWeatherLive, 2023)

Figure 8.1 shows that in the last winter (2022-2023), the "*obsigend*" phases twice correlate with icing. Even though it does not appear to be the case that every "*obsigend*" stage also forms ice in the stream or that "*nidsigend*" phase no ice formation occurs in the river despite cold temperatures, it is believed that this observation is considered an old farmer's rule and has been passed down from generation to generation.

Bibliography

Alfredsen, Knut, Bridges, Robert, et al. (2022). "How does climate change affect ice formationand presence in rivers, lakes and oceans,as well as its impact on infrastructure". In: *Climate Change*.

Alfredsen, Knut, Stickler, Morten, and Pennell, Curtis (2006). "Ice formation and breakup in steep streams". In: *Proceedings of the 18th IAHR International Symposium on Ice, Sapporo, Japan* 28.

Barry, Roger G. (1992). *Mountain Weather and Climate*. 2nd edition. London: Routledge. ISBN: 978-0-415-07113-0.

Beltaos, Spyros, ed. (2013). *River ice formation*. Edmonton, Alberta, Canada: Committee on river ice processes and the environment, Canadian geophysical union hydrology section. ISBN: 978-0-9920022-0-6.

Blackburn, Julia and She, Yuntong (2019). "A comprehensive public-domain river ice process model and its application to a complex natural river". In: *Cold Regions Science and Technology* 163, pp. 44–58. DOI: 10.1016/j.coldregions.2019.04.010.

Boyd, Sean, Ghobrial, Tadros, and Loewen, Mark (Jan. 2023). "Analysis of the surface energy budget during supercooling in rivers". In: *Cold Regions Science and Technology* 205, p. 103693. DOI: 10.1016/j.coldregions.2022.103693.

Boyd, Sean, Ghobrial, Tadros, Loewen, Mark, et al. (2022). "A study of supercooling in rivers". In: *Cold Regions Science and Technology* 194.103455. DOI: 10.1016/j.coldregions.2021.103455.

Buffin-Bélanger, Thomas, Bergeron, Normand E, and Dubé, Jérôme (2013). "River ice formation in small rivers". In: *River ice formation*. Ed. by Beltaos, Spyros. Committee on River Ice Processes, the Environment, and Hydrology Section of the Canadian Geophysical Union, pp. 385–409.

BUWAL, Bundesamt für Umwelt Wald und Landschaft (2000). *Angemessene Restwassermengen: Wie können sie bestimmt werden?* Tech. rep.

Chen, Yunfei et al. (Jan. 2023). "Advances in Frazil Ice Evolution Mechanisms and Numerical Modelling in Rivers and Channels in Cold Regions". In: *Water* 15.14, p. 2582.

Daly, Steven F. (2013). "Frazil Ice". In: *River ice formation*. Beltaos, Spyros, pp. 107–133.

Davos, Gemeinde (2020). *Fertigstellung eines Revitalisierungsprojekts am Dischmabach*. URL: https://www.gemeindedavos.ch/newsarchiv/1013935 (visited on 06/14/2023).

Decentlab (2018). *DL-PR26 Datasheet*.

Dubé, Mathieu, Turcotte, Benoit, and Morse, Brian (2014). "Inner structure of anchor ice and ice dams in steep channels". In: *Cold Regions Science and Technology* 106-107, pp. 194–206. DOI: 10.1016/j.coldregions.2014.06.013.

Eberhard, Lucie A. et al. (2021). "Intercomparison of photogrammetric platforms for spatially continuous snow depth mapping". In: *The Cryosphere* 15.1, pp. 69–94.

Eubank, Randall L (1999). *Nonparametric Regression and Spline Smoothing*. 2nd. Vol. 157. Boca Raton: Marcel Dekker.

Fiorotto, Virgilio and Caroni, Elpidio (2013). "A new approach to master recession curve analysis". In: *Hydrological Sciences Journal* 58.5, pp. 966–975. DOI: 10.1080/02626667.2013.788248.

FOEN, Federal Office for the Environment (2021). "Effects of climate change on Swiss water bodies; Hydrology, water ecology and water management". In: *Environmental studies*.

— (2022). *Restwasser*. URL: https://www.bafu.admin.ch/bafu/de/home/themen/wasser/fachinformationen/massnahmen-zum-schutz-der-gewaesser/renaturierung-der-gewaesser/restwasser.html (visited on 09/28/2023).

— (2023). *Dischmabach - Davos, Kriegsmatten 2327*. URL: https://www.hydrodaten.admin.ch/de/2327.html (visited on 06/14/2023).

Frankhauser, Thomas (Dec. 2022a). *"Obschigend und Nidgschigend"*. Swiss German.

— (Oct. 2022b). *Eis im Bach*. Swiss German.

Gan, Rong, Sun, Lin, and Luo, Yi (May 2015). "Baseflow characteristics in alpine rivers — a multi-catchment analysis in Northwest China". In: *Journal of Mountain Science* 12.3, pp. 614–625. DOI: 10.1007/s11629-013-2959-z.

Ghobrial, T. R. and Loewen, M. R. (2021). "Continuous in situ measurements of anchor ice formation, growth, and release". In: *The Cryosphere* 15.1, pp. 49–67. DOI: 10.5194/tc-15-49-2021.

HADES (2023). *Hydrological Atlas of Switzerland, Data and Analysis Platform*. URL: https://hydromaps.ch/#en/12/46.7382/9.9100/bl_hds--a05_a05_20180118a_outlets_epsg2056$undefined+0/CH-0159 (visited on 06/14/2023).

Hirayama, Kenichi, Yamazaki, Makoto, and Tao Shen, Hung (2002). "Aspects of river ice hydrology in Japan". In: *Hydrological Processes* 16.4, pp. 891–904. DOI: 10.1002/hyp.375.

Kohler, Andreas (Oct. 2023). *Korrektur Pegelganglinien*. Swiss German.

Lamb, Robert and Beven, Keith (1997). "Using interactive recession curve analysis to specify a general catchment storage model". In: *Hydrology and Earth System Sciences* 1, pp. 101–113.

Lind, Lovisa et al. (2016). "Hydrological and thermal controls of ice formation in 25 boreal stream reaches". In: *Journal of Hydrology* 540, pp. 797–811. DOI: 10.1016/j.jhydrol.2016.06.053.

McFarlane, Vincent and Clark, Shawn P. (2021). "A detailed energy budget analysis of river supercooling and the importance of accurately quantifying net radiation to predict ice formation". In: *Hydrological Processes* 35.3.

Nafziger, Jennifer et al. (2017). "Anchor ice formation and release in small regulated and unregulated streams". In: *Cold Regions Science and Technology* 141, pp. 66–77. DOI: 10.1016/j.coldregions.2017.05.008.

Pan, Jiajia, Shen, Hung Tao, and Jasek, Martin (2020). "Anchor ice effects on river hydraulics". In: *Cold Regions Science and Technology* 174.103062. DOI: 10.1016/j.coldregions.2020.103062.

Posavec, Kristijan, Giacopetti, Marco, and Birk, Steffen (2017). "Method and Excel VBA Algorithm for Modeling Master Recession Curve Using Trigonometry Approach". In: *Groundwater* 55.6, pp. 891–898.

Prowse, Terry D. (2001). "River-Ice Ecology. I: Hydrologic, Geomorphic, and Water-Quality Aspects". In: *Journal of Cold Regions Engineering* 15.1, pp. 1–16. DOI: 10.1061/(ASCE)0887-381X(2001)15:1(1).

Qu, Y X and Doering, J (2007). "Laboratory study of anchor ice evolution around rocks and on gravel beds". In: *Canadian Journal of Civil Engineering* 34.1, pp. 46–55. DOI: 10.1139/l06-094.

Schaefli, B., Rinaldo, A., and Botter, G. (2013). "Analytic probability distributions for snow-dominated streamflow". In: *Water Resources Research* 49.5, pp. 2701–2713. DOI: 10.1002/wrcr.20234.

schweizerfluss.ch (2023). *Dischmabach*. URL: https://schweizerfluss.ch/dischmabach/.

Smakhtin, V. U (Jan. 2001). "Low flow hydrology: a review". In: *Journal of Hydrology* 240.3, pp. 147–186. DOI: 10.1016/S0022-1694(00)00340-1.

SpaceWeatherLive (2023). *Moon Phase Calendar*. URL: https://www.spaceweatherlive.com/en/moon-phases-calendar.html.

Stickler, Morten and Alfredsen, Knut T. (2009). "Anchor ice formation in streams: a field study". In: *Hydrological Processes* 23.16, pp. 2307–2315. DOI: 10.1002/hyp.7349.

Stoelzle, M., Stahl, K., and Weiler, M. (Feb. 2013). "Are streamflow recession characteristics really characteristic?" In: *Hydrology and Earth System Sciences* 17.2, pp. 817–828. DOI: 10.5194/hess-17-817-2013.

Strohmenger, Laurent et al. (2023). "On the visual detection of non-natural records in streamflow time series: challenges and impacts". In: *Hydrology and Earth System Sciences* 27.18, pp. 3375–3391. DOI: 10.5194/hess-27-3375-2023.

Swisstopo (2023a). *Geoportal des Bundes: Chriegsmatten, Dischmatal, Davos*. URL: map.geo.admin.ch (visited on 06/14/2023).

— (2023b). *Landschaftsmodelle*. URL: https://www.swisstopo.admin.ch/de/geodata/landscape.html (visited on 12/07/2023).

Tallaksen, L.M. (1995). "A review of baseflow recession analysis". In: *Journal of Hydrology* 165, pp. 349–370.

Terada, Koichiro, Hirayama, Kenichi, and Sasamolo, Makolo (1999). "Field measurement of anchor and frazil ice". In: *Ice in Surface Water*. Rotterdam: Shen.

Turcotte, Benoit and Morse, Brian (2013). "A global river ice classification model". In: *Journal of Hydrology* 507, pp. 134–148. DOI: 10.1016/j.jhydrol.2013.10.032.

Verbunt, M. et al. (2003). "The hydrological role of snow and glaciers in alpine river basins and their distributed modeling". In: *Journal of Hydrology* 282.1, pp. 36–55. DOI: 10.1016/S0022-1694(03)00251-8.

Walter-Degener, Brigitte (2017). *Dischmatal, Bilder, Geschichten, Rezepte*. Buschhausen: Druck- & Verlagshaus Herten. ISBN: 978-3-946030-47-8.

wingtra (2023a). *Sony RX1R II*. URL: https://wingtra.com/mapping-drone-wingtraone/mapping-cameras/sony-rx1r-ii/ (visited on 08/19/2023).

— (2023b). *WingtraOne GEN II*. URL: https://wingtra.com/mapping-drone-wingtraone/ (visited on 08/19/2023).

Chapter 9

Appendix

9.1 Stream width calculation pseudocode

```
# Create points along the central line
points = [central_line.interpolate(i * distance_between_points)
for i in range(num_points)]

# Create an empty GeoDataFrame for the perpendicular lines
perpendicular_lines = gpd.GeoDataFrame(columns=['geometry'])

# Create perpendicular lines at each point for point in points:
    # Calculate the azimuth (angle) for the perpendicular line:
        (90 degrees for vertical)
        azimuth = 90
    # Calculate the coordinates for the endpoint of the perpendicular line:
        x = point.x + distance_between_lines *
            (distance_between_points / 2) *
            (1 if azimuth == 90 else -1)
        y = point.y + distance_between_lines *
            (distance_between_points / 2) *
            (0 if azimuth == 90 else 1)
    # Create the perpendicular line:
        perpendicular_line = LineString([point, Point(x, y)])
    # Add the line to the GeoDataFrame:
         perpendicular_lines =
            perpendicular_lines.append({'geometry': perpendicular_line},
            ignore_index=True)
```

9.2 Event characterisation

ID	date	air_temp				water_temp				Q m^3/s				meteo		comment
		date -1 16:00	date 00:00	date 07:00	date 12:00	date-1 16:00	date 00:00	date 07:00	date 12:00	date-1 16:00	date 00:00	date 07:00	date 12:00	meteo_daybefore	meteo	
1	06.12.22	-3.4	-7.6	-8.7	-2.1	1.4	0.08	0.05	0.16	0.796	0.765	0.728	0.857	light snowfall	sunny	
2	07.12.22	-3.9	-7.1	-8.2	-2	0.51	0.08	0.07	0.17	0.77	0.754	0.742	0.78	sunny	sunny	
3	12.12.22	-11.7	-15.9	-15.7	-7.4	0.39	0	0	0.13	0.725	0.604	0.615	0.726	cloudy	sunny	
4	18.01.23	-2.2	-9.2	-9.1	-3.7	0.67	0.07	0.12	0.23	0.556	0.504	0.521	0.604	sunny	sunny	
5	08.02.23	-5.1	-12.6	-13.4	-3.9	0.13	0.05	0.02	0.28	0.484	0.321	0.35	0.591	sunny	sunny	Ice cover on top present
6	09.02.23	-4.4	-12.4	-15	-3.6	0.06	0.04	0.04	0.34	0.54	0.352	0.324	0.576	sunny	sunny	Ice cover on top present
7	10.02.23	-4.8	-12.6	-14.3	-1.2	0.09	0.07	0.07	0.38	0.55	0.356	0.371	0.617	sunny	sunny	Ice cover on top present
8	27.02.23	-7.8	-9.7	-8.5	-2.3	1.05	0.17	0.17	0.75	0.451	0.419	0.397	0.478	cloudy	sunny	Ice cover on top present
9	28.02.23	-4.4	-7.7	-8.8	1.7	2.05	0.12	0.15	1.22	0.455	0.419	0.337	0.484	sunny	sunny	
10	01.03.23	1	-6.5	-8.5	2.8	2.13	0.11	0.14	0.66	0.454	0.396	0.317	0.61	sunny	sunny	
11	03.03.23	4.1	-4.5	-6.1	3.1	3.98	0.96	0.19	2.38	0.436	0.428	0.364	0.512	sunny	sunny	
12	04.03.23	1.9	-3.8	-7.3	2.7	3.06	1.43	0.15	2.54	0.437	0.428	0.378	0.496	sunny	sunny	
13	05.03.23	2.8	-3.4	-7.6	3.5	3.09	0.71	0.09	1.19	0.433	0.425	0.302	0.598	sunny	sunny	
14	06.03.23	1.7	-6.4	-6.1	0.9	2.33	0.11	0.23	1.09	0.438	0.375	0.322	0.549	sunny	sunny	
15	16.03.23	-2.9	-6.6	-7.4	7.9	3.67	0.22	0.17	1.85	0.456	0.403	0.274	0.608	sunny	sunny	ice cover is broken
Statistics																
	Total winter															
	MIN	-11.70	-15.90	-15.70	-7.40	0.06	0.00	0.00	0.13	0.43	0.32	0.27	0.48			
	MAX	4.10	-3.40	-6.10	7.90	3.98	1.43	0.23	2.54	0.80	0.77	0.74	0.86			
	MEAN	-2.61	-8.40	-9.65	-0.24	1.64	0.28	0.11	0.89	0.53	0.46	0.42	0.61			
	ST. DEV	4.13	3.51	3.14	3.78	1.32	0.40	0.07	0.78	0.12	0.13	0.15	0.10			
	Early winter															
	MIN	-11.70	-15.90	-15.70	-7.40	0.06	0.00	0.00	0.13	0.45	0.32	0.32	0.48			
	MAX	-2.2	-7.1	-8.2	1.7	2.05	0.17	0.17	1.22	0.796	0.765	0.742	0.857			
	MEAN	-5.30	-10.53	-11.30	-2.72	0.71	0.08	0.08	0.41	0.59	0.50	0.49	0.63			
	ST. DEV	2.67	2.82	3.01	2.31	0.64	0.05	0.05	0.34	0.13	0.16	0.16	0.12			
	Late winter															
	MIN	-2.90	-6.60	-8.50	0.90	2.13	0.11	0.09	0.66	0.43	0.38	0.27	0.50			
	MAX	4.1	-3.4	-6.1	7.9	3.98	1.43	0.23	2.54	0.55	0.428	0.397	0.617			
	MEAN	-0.93	-6.80	-8.29	2.12	2.38	0.43	0.15	1.34	0.46	0.41	0.34	0.55			
	ST. DEV	3.89	2.77	2.32	2.77	1.17	0.46	0.05	0.72	0.03	0.02	0.04	0.06			

Figure 9.1: Characterization table of all the events found by the wildlife camera and additional statistics to define the threshold values for the Event-Finding-Algorithm divided into early (blue) and late (orange) winter

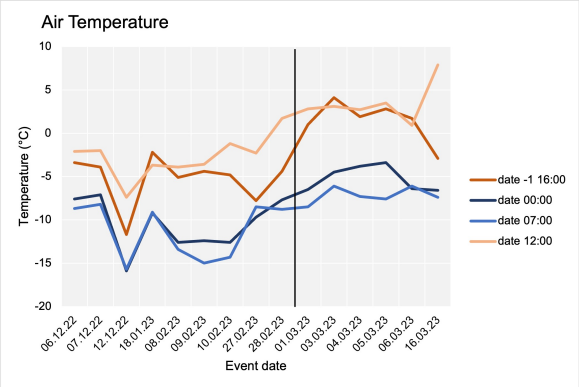

Figure 9.2: Air temperature ranges over the events found by the wildlife camera at different times during the day

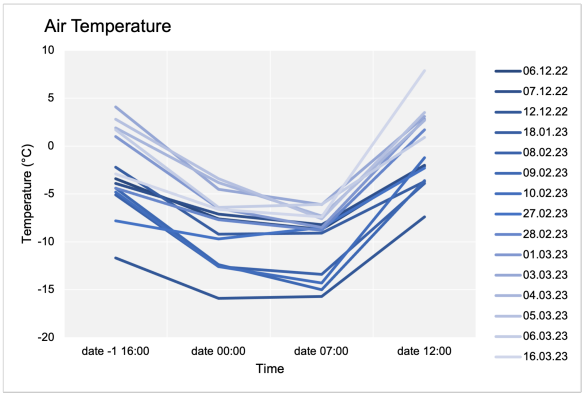

Figure 9.3: Air temperature ranges over the events found by the wildlife camera at different times during the day, and the vertical line marking the change from early to late winter

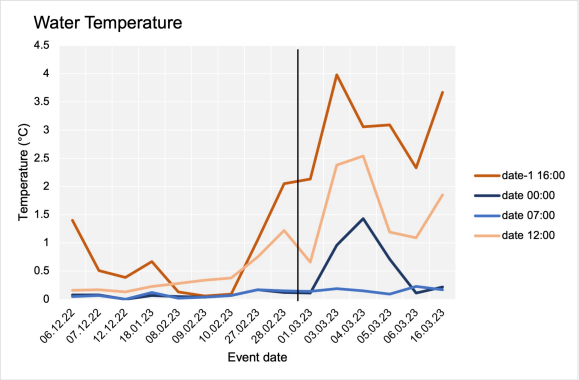

Figure 9.4: Water temperature ranges over the events found by the wildlife camera at different times during the day, and the vertical line marking the change from early to late winter

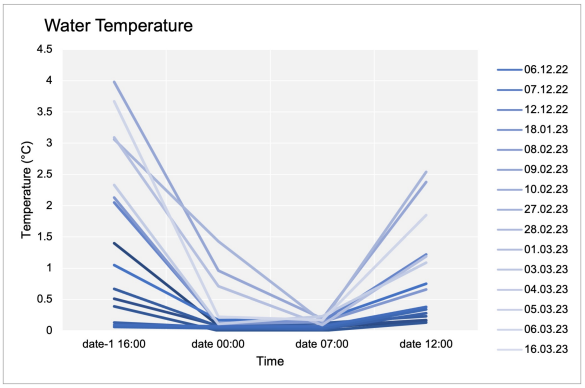

Figure 9.5: Water temperature over different times during the day forthe events found by the wildlife camera

9.3 Event extraction pseudocode

9.3.1 *Smooth spline* No-Ice-Model

```
1. model_smoother(data):
    a. Convert the date column to a datetime format.
    b. Initialize an empty results data frame.
    c. Loop over winters from 2004 to 2022:
        i. Define winter start and end dates.
        ii. Subset the data for that winter.
        iii. If no data exists for that winter, continue to the next.
        iv. Assign an ID sequence to the subsetted data.
        v. Fit a smooth spline model.
        vi. Join the results with the original data.
```

d. Return the joined data.

2. event_extraction(data, season):
    a. Set water and air temperature thresholds based on the input season.
    b. Calculate the slope of the discharge.
    c. Initialize a list for oscillation segments.
    d. Loop through the data to detect events based on multiple criteria,
    like water temperature, air temperature, discharge trends, etc.
    e. Return the detected segments as a list.

3. calculate_intersection(segments):
    a. For each segment in the list:
        i. Calculate the slope and intercept for discharge and the model.
        ii. Find the intersection point between the discharge
        and model curves.
    b. Return the intersection points as a list.

4. calculate_volumes(segments, intersection_points):
    a. For each segment in the list:
        i. Calculate the volume using the area between the model
        and discharge.
        ii. Calculate other related metrics such as the mean volume loss
        and the expected discharge.
    b. Return the calculated volumes as a data frame.

9.3.2 *Exponential decay* No-Ice-Model

1. event_extraction(data, season):
    a. Set water and air temperature thresholds based on the input season.
    b. Calculate the slope of the discharge.
    c. Initialize a list for oscillation segments.
    d. Loop through the data to detect events based on multiple criteria,
    like water temperature, air temperature, discharge trends, etc.
    e. Add no-ice model for every found event
        i. Set 'dbe' to 'pretime + 1' which signifies hours before the event.
        ii. Extract a segment of data from 'j - pretime' to 'j + 48',
        this represents a x-day segment.
        iii. Assign a sequence of numbers as ID to the extracted segment.
        iv. Build an exponential model (using a natural logarithm
        transformation)

to describe the discharge without icing events.

v. Compute the model prediction for the segment.

f. Store the segment in the 'segments' list with a date-based key.

g. Return the detected segments as a list.

3. calculate_intersection(segments):

a. For each segment in the list:

i. Calculate the slope and intercept for discharge and the model.

ii. Find the intersection point between the discharge and model curves.

b. Return the intersection points as a list.

4. calculate_volumes(segments, intersection_points):

a. For each segment in the list:

i. Calculate the volume using the area between the model and discharge.

ii. Calculate other related metrics such as the mean volume loss and the expected discharge.

b. Return the calculated volumes as a data frame.

Personal Declaration: I hereby declare that the submitted thesis results from my own independent work. All external sources are explicitly acknowledged in the Thesis.

Zurich, November 6, 2023

Nina Chiara Nagel